ISSN 2720-3581

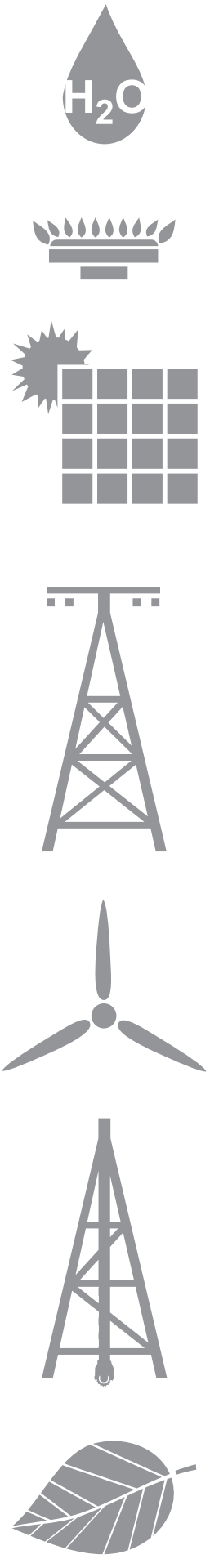

JOURNAL OF GEOTECHNOLOGY AND ENERGY

FORMERLY AGH DRILLING, OIL, GAS

2025, vol. 42, no. 2

WYDAWNICTWA AGH

KRAKOW 2025

The "Journal of Geotechnology and Energy" (formerly "AGH Drilling, Oil, Gas") is a quarterly published by the Faculty of Drilling, Oil and Gas at the AGH University of Krakow, Poland. Journal is an interdisciplinary, international, peer-reviewed, and open access. The articles published in JGE have been given a favorable opinion by the reviewers designated by the editorial board.

Editorial Team

Publisher

AGH University Press

Linguistic corrector: *Aeddan Shaw*
Technical editor: *Kamila Zimnicka*
Desktop publishing: *Munda*
Cover design: *Paweł Sepielak*

ISSN: 2720-3581
DOI: https://doi.org/10.7494/jge

Journal website: https://journals.agh.edu.pl/jge

Wydawnictwa AGH (AGH University Press)
al. A. Mickiewicza 30, 30-059 Kraków
tel. 12 617 32 28, 12 636 40 38
e-mail: redakcja@wydawnictwoagh.pl
www.wydawnictwo.agh.edu.pl

CONTENTS

Journal of Geotechnology and Energy | vol. 42 | no. 2 | 2025 | pp. 5–13

https://doi.org/10.7494/jge.2025.42.2.7002

ARTICLE

Radosław Hofman

Independent Researcher
ORCID: 0000-0001-5693-8151
e-mail: radoslaw@hofman.phd

ANALYSIS OF THE POSSIBILITY OF AN INCORRECT SHIFT OF THE MECHANICAL INDEX OF A DIAPHRAGM GAS METER WORKING UNDER VIBRATION

Date of submission:
22.02.2025

Date of acceptance:
10.04.2025

Date of publication:
30.06.2025

https://journals.agh.edu.pl/jge

Abstract: The article discusses the operation of bellows gas meters, commonly used to measure household gas consumption. It was noted that their testing and certification scope covers laboratory conditions, including work in vibration-free conditions, while vibrations occur in actual situations. It should be noted that the presented analysis is part of analyzing illegal gas consumption – UAG (unaccounted for gas), which is the subject of scientific research both in Poland and globally. The Oil and Gas Institute itself states [1] that it has received approximately 1,400 expert opinions, in which the gas meter user indicated that the counter had been skipped, while laboratory tests of the gas meter did not confirm any irregularities. The author, therefore, addresses the topic by asking whether the design of bellows gas meters with a mechanical counter may contain a design defect that may cause the counter to skip and then "disappear". As part of the research, an analysis was made of whether vibrations had any impact on the operation of the gas meter, and after confirming the implications, the counter was dismantled, and an attempt was made to determine the causes of the impact of vibrations. Finally, it was indicated what values of forces and acceleration are sufficient to cause measurement errors, and it was recommended that the construction of the counter be modified to prevent this phenomenon from occurring. The conclusions show that if the gas meter is used outside the scope of its certification, the counter may jump. Still, this jump will not leave any mechanical traces, and the gas meter may ultimately function appropriately after the vibrations stop.

Keywords: diaphragm gas meter, mechanical index, incorrect shift of gas meter index, illegal gas consumption, gas theft, unaccounted-gas lost, expertise

1. Introduction

In the gas distribution system, both in Poland and worldwide, bellows gas meters with a mechanical counter are most commonly used, especially for individual customers. A few years ago, there were about 8 million such gas meters in Poland [2–7]. One of the important aspects of using gas meters are errors reported by their users ("meter jumps"), which, although theoretically possible, could not be demonstrated in previous research studies either under what conditions they occurred or confirmed that they occurred at all [1]. In particular, the 2022 publication indicates a very laborious analysis performed by the authors, who examined a number of gas meters simulating approx. 10 years of gas consumption and did not notice the possibility of a jump, even despite hitting the meter with a force of up to 0.62 N [1].

The PN-EN 1359:2017 [8] standard for gas meters indicates that they are adapted to work in situations where vibrations and shocks are of little significance. However, to the best of the author's knowledge, no work has been carried out to answer the question of what vibrations of little significance mean.

In practical situations, gas installation pipes run under streets, which are often corrugated or have gaps in the roadway, and each passage of a heavy vehicle can cause vibrations that will be transferred to the meter through the gas installation pipes. Moreover, it happens that earthworks are carried out near the gas meter, including work using vibrating road rollers. Such rollers generate vibrations with a frequency of up to 50 Hz (3,000 cycles per minute) with an excitation of 2 mm, which means a direct interaction with an acceleration exceeding 24 times the value of the acceleration of gravity (g).

$$a = -A\,\omega^2 \sin(\omega\, t) \tag{1}$$

Substituting the parameters of the vibrating roller:

$$\omega = 55\ \text{Hz} \cdot 2 \cdot 3.14 = 345.4\ \text{rad/s} \tag{2}$$

$$a_{max} = 0.002\ \text{m} \cdot (345.4\ \text{rad/s})^2 = \\ = 238.6\ \text{m/s}^2 = 24.3\ g \tag{3}$$

Of course, the same acceleration will not be transferred to the gas meter in every case because it depends on the gas installation layout. However, in old buildings where gas meters are located in houses and not connections directly at the installation, vibrations may even be intensified due to the long arm of the force. The question therefore arises as to what type and what strength of vibrations go beyond vibrations of minor significance, and what elements of the gas meter or counter construction are susceptible to them.

2. First experiments

Building a device that would allow for obtaining target vibrations turned out to be a complex issue. The author planned the following arrangement of two gas meters, connected to an air flow source and a vibration source (Fig. 1).

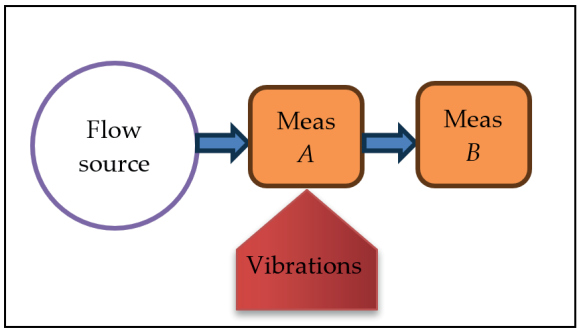

Fig. 1. Measurement schema

The compressed air was to flow first through gas meter A, subjected to vibrations, and then be pumped directly from it to gas meter B – identical and operating under normal conditions. In this way, the risk of leakage in the measuring system was eliminated (if it occurred, significantly lower readings would be obtained on gas meter A than on B with the vibration generator switched off) and the system was theoretically ensured to operate synchronously. Since the scope of the study was limited, it was assumed that any difference in the operation of both systems was to be measured in the absence of vibrations, and then it was expected that this difference would be constant despite the activation of the vibration generator. Ultimately, it would be necessary to consider carrying out these studies with a larger number of meters and a stable source of pumping air, however, the aim of the experiment was only to determine whether vibrations affect the operation of the gas meter or not, hence the precise effect of vibrations on the measurement value was not of fundamental importance.

Several vibration generating systems were assembled – using an exercise mat type generator (generating vibrations in two planes with a frequency of up to 50 Hz) and an electric saw (generating vibrations in one plane with a frequency of up to 50 Hz). It turned out that the strength of the test set itself was a rather complex issue, because at a given vibration frequency and mass inertia of the gas meter, very high stresses were obtained on the vibration transfer system. The physical implementation of the measuring system is shown in Figures 2 and 3, and the measurement results are in Table 1.

Fig. 2. Physical implementation of the measurement system based on an exercise mat (2D vibration)

Fig. 3. Physical implementation of the measurement system based on an electric saw (1D vibration)

Table 1. Meter readings during measurements

Type of vibrations	Meas. *A*	Measurements *B*	Delta *A*	Delta *B*	Relative error [%]	Error cum. [%]
No vibrations	0.195	0.231	–	–	–	–
	2.165	2.248	1.970	2.017	102.39	103.83
2D vibrations	3.764	3.886	1.599	1.638	102.44	103.24
	4.764	4.902	1.000	1.016	101.60	102.90
	5.915	6.073	1.151	1.171	101.74	102.67
	9.464	9.655	3.549	3.582	100.93	102.02
	12.954	13.180	3.490	3.525	101.00	101.74
	16.438	16.721	3.484	3.541	101.64	101.72
1D vibrations	17.371	17.671	0.933	0.950	101.82	101.73
	19.047	19.380	1.676	1.709	101.97	101.75
	21.027	21.394	1.980	2.014	101.72	101.75
	21.577	**21.981**	**0.550**	**0.587**	**106.73**	101.87
	22.429	22.855	0.852	0.874	102.58	101.90
	22.538	22.965	0.109	0.110	100.92	101.89
	23.678	24.129	1.140	1.164	102.11	101.90
	24.675	25.142	0.997	1.013	101.60	101.89
	25.995	26.476	1.320	1.334	101.06	101.85

The measurement results indicate that meter *B* measured 2.39% more gas volume than meter *A* in the test without vibrations – this is surprising in itself, because this meter was connected in serial connection after meter *A*, and therefore it was to be expected that the measurement on this meter would be rather smaller (due to possible leaks). This may indicate a difference between the meters themselves, which, although purchased from the manufacturer's distribution network, were nevertheless delivered in a way that did not protect them from vibrations during transport. However, since the measurement difference in this direction could not have resulted from a leak in the system, it was decided to continue the study (Fig. 3, 4).

Subsequent measurements indicated a fluctuating value of the relative error from 0.92% to 2.44% of the measured volume, while one of the measurements indicated an error of 6.73%. The measurements do not indicate what the relationship was between specific vibrations and a specific error value, but it was certainly possible to demonstrate that vibrations of the order of 50 Hz disturb the operation of the meter.

Interestingly, the phenomenon of waving the digits of the abacus was observed – during single-plane horizontal vibrations from the direction shown in Figure 4 and when the vibrations were transferred in such a way that the abacus was subject to vibrations, the drums of the abacus moved up and down by about 3 mm on their own – this did not cause the drums to jump, but indicated that the jump would have occurred if the drum had not been stopped by the decade flip-flop.

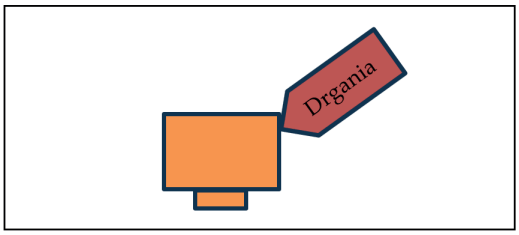

Fig. 4. Direction of vibrations at which the "waving" phenomenon of the counter drums was observed

The results of the above experiments and measurements are of course not definitive, therefore it was decided to conduct further analyses after dismantling the counter.

3. Dismantling the counter

The dismantling of the abacus was done in a non-standard way – it was decided to cut out the abacus glass and cut the fasteners using an angle grinder to ensure that the abacus could be removed without any shifting that could change its condition during dismantling (Fig. 5).

Immediately after cutting off the abacus, the phenomenon that we tried to demonstrate was observed, namely – almost all of the abacus drums could be turned freely. The protection in the form of decade flip-flops did not hinder this rotation in any way. After a preliminary analysis of the phenomenon, it was recorded on film.

It was therefore necessary to explain the cause of this phenomenon – as a reminder, it should be added that the counter was working properly just before dismantling (apart from a momentary deviation during one measurement), but after dismantling the counter, it turned out that the protections for the free rotation of the drums did not work.

After analyzing the condition of the counter, the pin on which the counter drums are mounted was observed to have been pushed out.

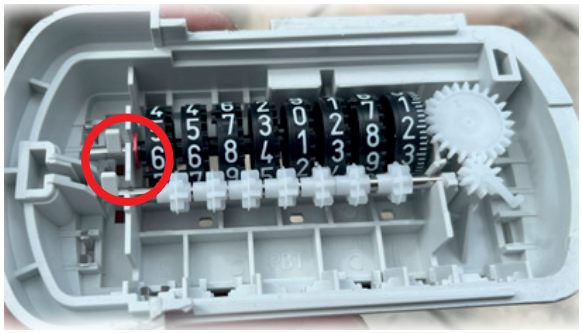

Fig. 6. Extension of the pin on which the counter drums are mounted

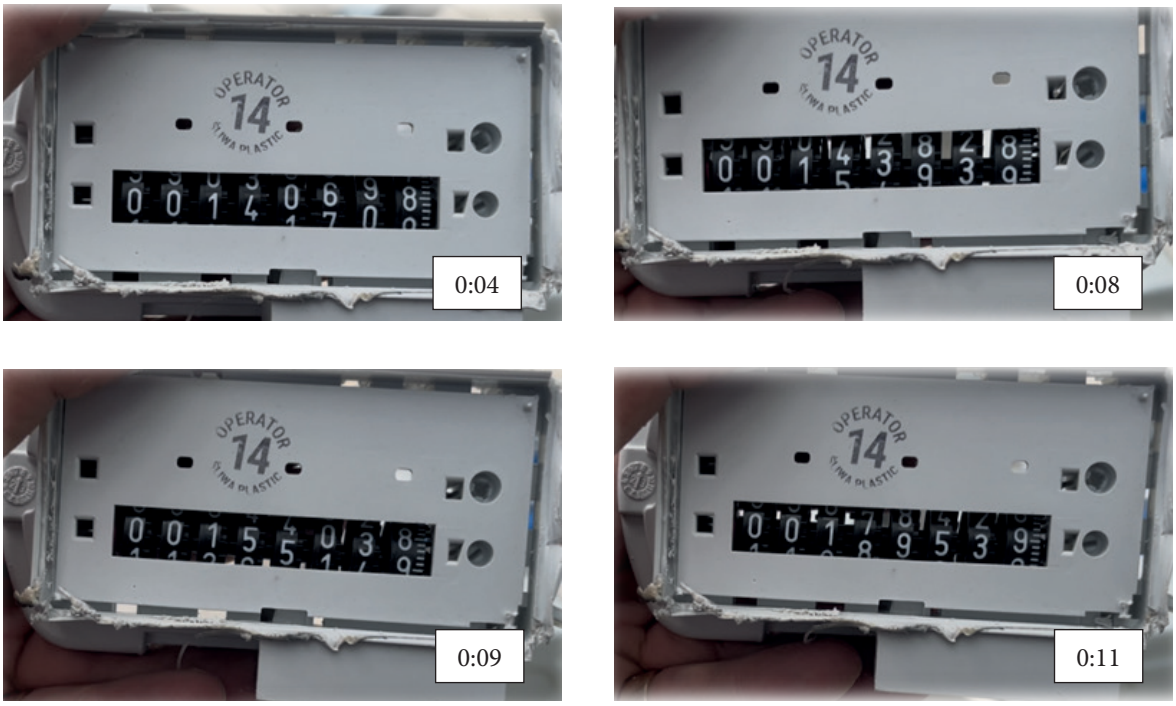

Fig. 5. Selected frames of a film showing the free rotation of the abacus drums

The pin in this position prevented the drums from adhering to the decade flip-flops and allowed them to rotate freely. It should be added that the greatest impact of the extension has on the drums located on the opposite side of the counter (the liter digit), while in relation to the drum located at the very extension, the distance from the decade flip-flop is too small to be able to rotate freely. In other words, all drums are subject to free rotation, up to and including the hundreds-cubic-meter digit, while the thousands-cubic-meter digit already shows elements of resistance, while the tens of thousands-cubic-meter digits cannot be rotated freely (Fig. 6).

After setting the pin in its correct position, the counter continued to work correctly, but there were no traces of mechanical skipping anywhere on it, because it took place on the principle of the free rotation of the drums. What is also important – all the movable drums could be rotated freely forwards, while the drums on the far right (located farthest from the extension) could be rotated in both directions. This way, if the phenomenon occurred under actual operating conditions, it would be more likely to result in an overestimated reading.

4. The jump of the abacus

Taking into account the influence of the extended pin of the counter drums on the correctness of the work, it was decided to investigate what force (acceleration) is sufficient to extend it. For this purpose, an Extech VB300 vibrometer was used, which allows for measuring acceleration in 3 planes (Fig. 7).

The cut off counter, with the pin inserted into the correct position, was placed on a plane, and then the vibrometer was struck on the counter with a small force. As a result of the impact, the pin extended by 0.5 mm.

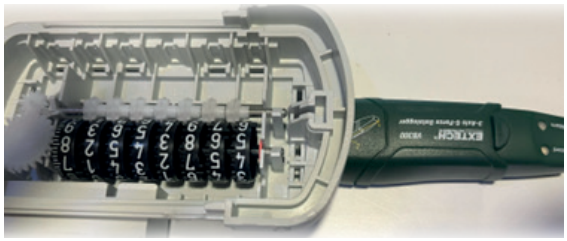

Fig. 7. Extension of the pin on which the counter drums are mounted

An acceleration of around 8 g may seem large, but it is an acceleration of impact. Comparable experiments were performed and a pen falling from a height of about 60 cm caused an acceleration of around 6 g to be recorded. It should also be remembered that when a vibrating cylinder is working, at a frequency of 50 Hz and a forcing of 2 mm, the acceleration is 24 g. The author therefore considers that an instantaneous acceleration at the moment of impact of around 8 g indicates a rather small force of impact (Fig. 8).

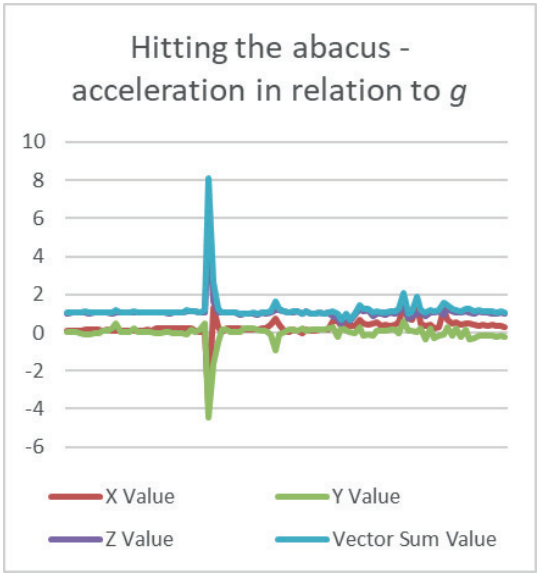

Fig. 8. Acceleration value at the moment of impact – readings every 50 ms

Using Newton's second law of dynamics and assuming that the drum pin weighs 2 g, an acceleration of 8 *g* is obtained with a force of $F = 0.14$ N. This force is sufficient to extend the pin by about 0.5 mm. This is a surprisingly small value – it is a force comparable to the force of gravity acting on an AAA battery.

Further experiments have shown that when the pin is extended by 2 mm (i.e. after four similar strikes), the first drums are moved away from the decade flip-flops, which can also be manifested by the lack of contact between the drum teeth and the gear wheel driving the counter (Fig. 9).

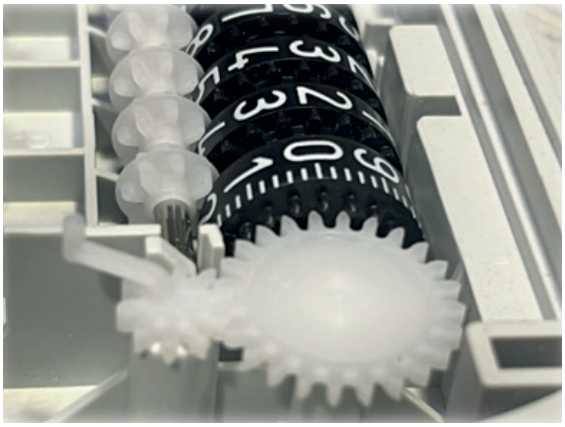

Fig. 9. Deflection of the drums after extending the pin by 2 mm

When the pin is fully extended (above 5 mm) all the drums can be turned freely (apart from the ones closest to the point of extension, which was discussed earlier). Of course, once the pin is pushed back into place, the counter works properly again and there is no trace of the skip on the drums.

5. Spreading the drums

The above analyses, although indicating that the meter is not adapted to work in vibration conditions, do not indicate the possibility of overestimating the gas reading, but rather underestimating it. Is there therefore a mechanical possibility of overestimating the reading?

Further analyses were carried out and it was determined that the nominal distance between the drums is 2 mm, the width of the tooth in the drum is about 1.3 mm, and the decade flip-flops have alternating teeth of 3 mm and 4 mm width. The principle of operation is such that the wider tooth of the decade flip-flop comes into contact with the protruding tooth of the lower digit, which rotates it by the distance of the larger and smaller tooth, which in turn causes the "older" drum to move by two teeth, i.e. exactly the distance needed to move by one digit (Fig. 10–14).

However, the drums have some freedom to deviate from the plane of rotation (due to the clearances between the pin constituting the axis of rotation and the inner diameter of the drum). In the tested abacus, a distance of 3 mm (1 mm more than the nominal distance) can be obtained without using any significant force.

It should be noted that in the case of this new distance increased by the depth of the tooth in the drum (1.3 mm) gives a total of 4.3 mm, which is enough space for the larger tooth of the decade flip-flop to fall into this space and then move the drum regardless of the fact that the number 9 has not yet appeared on the "younger" drum. Interestingly, this phenomenon can only occur for drums whose "younger" drum is set to at least the number 1 (it will not occur on drums whose "younger" drum is set to the number 0, due to the position of the protruding tooth of this "younger" drum).

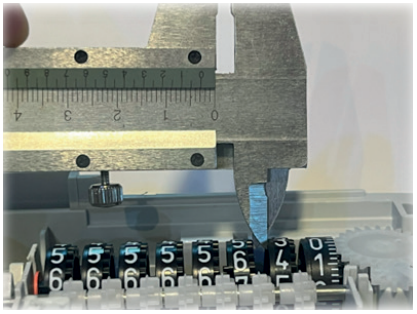

Fig. 10. Possible opening of the drums is 3 mm

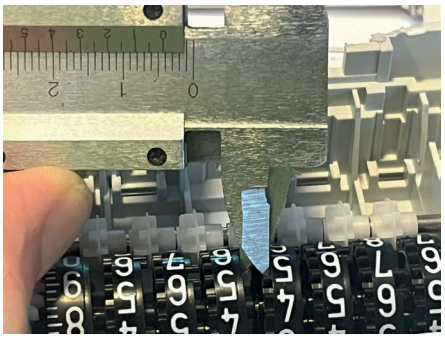

Fig. 11. The distance from the drum to the tooth cavity (4.30 mm)

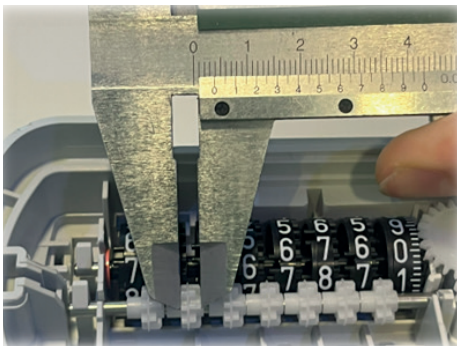

Fig. 12. The width of the wider tooth of the decade flip-flop (4 mm)

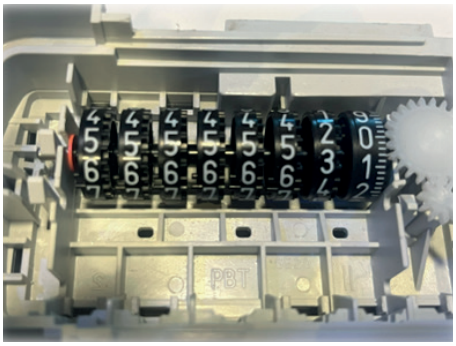

Fig. 13. The position of the teeth initiating the shifting of the "older" drum for drums indicating the number 0

Fig. 14. Indication of the abacus at the beginning of the test

Fig. 15. Correct arrangement of the teeth of the decade flip-flops on the drums

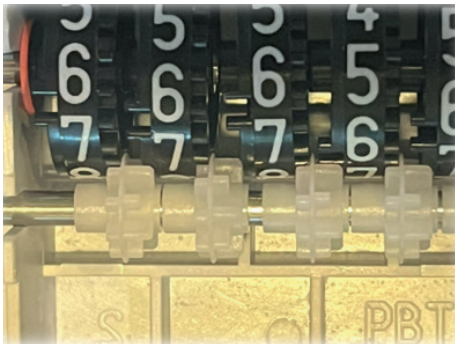

Fig. 16. Possibility of the slip-up of the wider tooth of the decade flip-flop into the space between the drums

Fig. 17. Wider tooth of the decade flip-flop inserted between drums during rotation

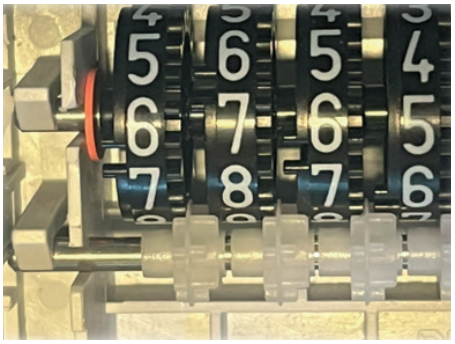

Fig. 18. New position of the drums and no signs of skipping

Fig. 19. New indication of the abacus

It is obvious that the probability of the drums spontaneously moving apart and the wider tooth of the decade flip-flop falling between these drums is negligible. However, taking into account the long time horizon (vibrations lasting for weeks), this probability increases. Importantly, it was possible to demonstrate that the abacus jump is possible. Due to the manufacturer's designed drum clearances and the dimensions of the teeth, at the moment of the drums moving apart there is still 0.3 mm of reserve, and therefore the tooth of the decade flip-flop can fit in the space between the drums and move the "older" drum without using additional force. Importantly, the abacus jump does not leave any mechanical traces on the drums and decade flip-flops (Fig. 15–19).

It should be added that after the experiment was completed, the abacus was also dismantled in the second counter – the one that was not subjected to vibrations. It turned out that in this counter, moving the spindle on which the counter drums are mounted is much more difficult (no precise measurements were made), from which the conclusion is that long-term vibrations can not only be the cause of the spindle displacement itself, but also cause an increase in the clearance between the spindle and the drums, which facilitates any potential displacement.

6. Conclusions

Finally, it was decided to use the conclusions from the analyses from the previous points on the second, undissembled gas meter. It was connected to a system that pumped 0.240 m^3 of air through it in 30 seconds, and then the gas meter was hit several times with a hammer (through pliers, so as not to damage the casing) on the side of the counter from the side of the driving digits. The blows were quite strong – as earlier experiments showed, the extension of the pin occurred at an acceleration of around 8 g. With a mass of the gas meter

with a connected cable of around 5 kg, an acceleration of 8 g can be obtained by applying a force of 400 N (corresponding to the force of gravity acting on a weight of 40 kg). The force of the impact was much smaller, although its value was not determined, however, it did not have a significant event, because the purpose of the impacts was to reproduce the effect that vibrations acting for many hours can have on the gas meter, for which, as already mentioned, accelerations of up to 24 g can be expected. It can be assumed that achieving the intended effect rather indicates that in practice much less acceleration than 8 g is needed to extend the stem.

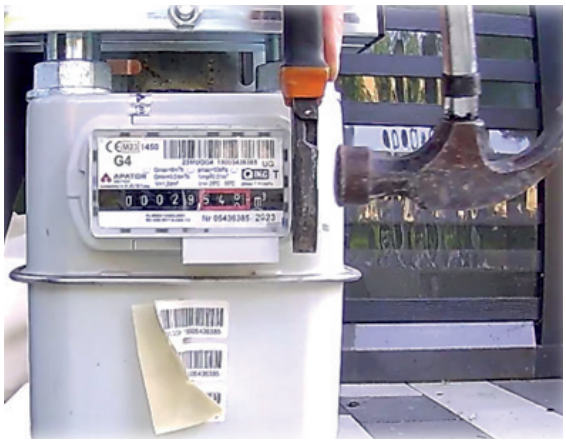

Fig. 20. A hammer blow simulating hours of vibration

As a result of the impact, the pin on which the drums are mounted moved completely. It is to be expected that many hours of vibrations cause the pin to gradually extend, so there are many intermediate states between the correct state and complete extension, but the aim of this final demonstration was to determine how the gas meter will behave after the pin is moved.

It turned out that the impact caused the entire pin with the drums to fall into the counter, and it was set in the correct position using a magnet to reproduce the state that would occur when the pin was gradually extended.

In the event of the effects of gas meter vibrations, the phenomenon of the entire pin retracting will most likely not occur, because the vibrations will gradually extend the pin until it is completely loose, but will still be in a position close to the initial one. As previous analyses have shown, extending the pin by about 2 mm is enough to start observing non-deterministic operation of the meter. What's more, since vibrations are usually oscillatory, the extended pin may reduce its extension as a result of further vibrations (Fig. 20).

A film was then recorded to show how the gas meter works. The film shows that the drums move almost simultaneously, so the counter jumps. This gas meter was not disassembled to leave it in a faulty state, despite having the original seals, but taking into account the description of the causes of the phenomenon in the previous chapters, it should be expected that there are no traces of jumps on the drums and decade flip-flops because they work in conditions of no pressure between these elements (Fig. 21).

Fig. 21. Selected frames showing the counter jumping in a sealed gas meter

The final conclusion is as follows: a jump of the counter of a bellows gas meter with a mechanical counter is possible when used in conditions of intense vibration.

Moreover, even if the gas meter were equipped with an electronic pulse counter, it would still have an incorrect reading, with the mechanical counter indicating an overstated value and the electronic counter indicating an understated value, due to the disconnection of the drive drum from the gear rotating the counter (pulses are counted based on the revolutions of the first drum).

It should also be added that manufacturers of meters can protect them from the effects described in this article. Firstly, by installing an element that prevents the shaft on which the drums are located from moving. Such an element can be installed after the counter is mounted (with a latch), or by extending the

elements securing the counter glass. Secondly, it is necessary to ensure that the drums are spread apart, even with the use of a small force, less than the wider tooth of the decade flip-flop. This can be achieved by mounting the drums on rolling bearings, for example (the current mounting method resembles a sliding bearing, hence the need to provide clearances). And thirdly – after making these modifications, full certification tests must be carried out to allow the meters to operate in vibration conditions.

Without the above modifications, readings of gas meters taken in operating conditions that exceed the scope of their certification described in the PN-EN 1359:2017 standard mean that these readings may be unreliable.

Funding: This research received no external funding.

Conflicts of Interest: The authors declare no conflicts of interest.

References

[1] Lipka T., Dudek A.: *Wstępna analiza możliwości przeskoku liczydła mechanicznego gazomierza miechowego*. Nafta-Gaz, 78, 7, 2022, pp. 535–541. https://doi.org/10.18668/NG.2022.07.05.
[2] Dudek A., Jaworski J.: *Wpływ warunków temperaturowych otoczenia na wymianę ciepła w przemysłowych gazomierzach miechowych*. Nafta-Gaz, 73, 5, 2017, pp. 321–331. https://doi.org/10.18668/NG.2017.05.04.
[3] Matusik J., Jaworski J.: *Optymalny dobór gazomierzy miechowych przez operatora systemu gazowniczego.* Nafta-Gaz, 73, 4, 2017, pp. 274–286. https://doi.org/10.18668/NG.2017.04.08.
[4] Dudek A.: *Wpływ warunków środowiskowych i instalacyjnych na proces wymiany ciepła w wybranych przemysłowych gazomierzach miechowych*. Nafta-Gaz, 76, 11, 2022, pp. 828–836. https://doi.org.10.18668/NG.2020.11.08.
[5] Gacek Z., Jaworski J.: *Optimisation of measuring system construction in the context of high flow variability*. Journal of Natural Gas Science and Engineering, 81, 2020, pp. 103447. https://doi.org/10.1016/j.jngse.2020.103447.
[6] Lipka T.: *Internet of Things (IoT) – LoRaWAN w praktyce.* Nafta-Gaz, 76, 2, 2020, pp. 119–124. https://doi.org/10.18668/NG.2020.02.06.
[7] Kułaga P.: *Nielegalny pobór gazu – ogólna charakterystyka*. Nafta-Gaz, 77, 4, 2021, pp. 270–278. https://doi.org/10.18668/NG.2021.04.07.
[8] PN-EN 1359:2017: *Gas meters. Bellows gas meters*, 2017.
[9] *Act of 10 April 1997: Energy Law*. Journal of Laws [Dz.U.] 1997 no. 54 item 348, consolidated text: Journal of Laws 2021, item 716, as amended.

Journal of Geotechnology and Energy | vol. 42 | no. 2 | 2025 | pp. 15–27

https://doi.org/10.7494/jge.2025.42.2.5837

ARTICLE

Remigiusz Kunasz

AGH University of Krakow, Faculty of Drilling, Oil and Gas, Poland
ORCID: 0009-0000-3875-0630
e-mail: kunasz@agh.edu.pl

Tomasz Śliwa

AGH University of Krakow, Faculty of Drilling, Oil and Gas, Poland
ORCID: 0000-0002-2728-3413
e-mail: sliwa@agh.edu.pl

Aneta Sapińska-Śliwa

AGH University of Krakow, Faculty of Drilling, Oil and Gas, Poland
ORCID: 0000-0002-7005-8190
e-mail: ans@agh.edu.pl

THE CONCEPT OF A DEEP BOREHOLE HEAT EXCHANGER AT THE AGH UNIVERSITY STUDENT CAMPUS

Date of submission:
28.11.2023

Date of acceptance:
12.06.2024

Date of publication:
30.06.2025

https://journals.agh.edu.pl/jge

Abstract: The paper provides an introduction to deep borehole heat exchangers, their use and completed projects worldwide. The aim of the study is to design a deep borehole heat exchanger at the AGH University Campus, more specifically its design, casing and internal heat exchanger pipe concept with a view to minimizing temperature losses. It goes on to describe the location of the project, including the geology of the area and the solution to the design problem, i.e. the casing of the borehole and the design concepts for the deep borehole heat exchanger. In the following section, the design of a deep borehole heat exchanger is presented. During the research, the main problem was the limited availability of articles on deep borehole heat exchangers. This is due to the continuous development and testing of new engineering ideas and the high implementation costs compared to the energy effects obtained. The publication only deals with technical issues, financial issues were not considered, among other things due to the current global geopolitical situation in 2023.

Keywords: deep borehole heat exchanger, geoenergetics, geothermal, drilling, geothermal heat pumps

1. Introduction

Nowadays, there is growing interest in energy from renewable sources due to an increase in public awareness of environmental issues or ensuring energy neutrality. More recently, the construction industry has been following the idea of creating buildings that consume less energy. Regardless of this, its sources are also changing. This can be achieved using, for example, thermal energy from the Earth's interior. This can be exemplified by deep borehole heat exchangers, which can operate independently, or shallow heat exchangers cooperating with geothermal heat pumps.

The aim of this paper is to design a deep borehole heat exchanger at the AGH University Student Campus in Krakow and to adapt the parameters of the operation of the system with a geothermal heat pump to the required average power needed to meet the energy demand for central heating and domestic hot water of selected dormitories.

The introduction introduces the concept of geothermal energy, ways of utilizing and accessing thermal energy in the rock mass, explains the operational principles of deep borehole heat exchangers and supplies some examples. The operational principles of geothermal heat pumps is also described. The research problem was then defined and the location of the proposed project was outlined along with the expected geological structure. In the next section, the design of a deep borehole heat exchanger is presented.

Due to increasing energy consumption in the world, mankind is being forced to look for new, alternative sources and ways of obtaining it. The reason for this is the depletion of classical energy resources and their negative impact on the environment [1].

1.1. The concept of the deep borehole heat exchanger

There is currently considerable interest in borehole heat exchangers around the world. The vast majority of these are shallow boreholes with depths of tens to hundreds of meters. The use of deep boreholes (e.g. with depths of 2,000 to 4,000 m) for the installation of deep borehole heat exchangers makes it possible to obtain higher working fluid temperatures and also more energy [2]. In contrast to shallow installations, a deep borehole heat exchanger is only able to convert energy for heating purposes. Due to the high rock temperatures in the rock mass, it is not advisable to use such exchangers for cooling purposes. Given the high costs of drilling boreholes, existing boreholes that were drilled for other purposes, such as negative exploration boreholes or depleted oil wells, are usually considered for investment [3].

1.2. Examples of deep borehole heat exchangers worldwide

To date, deep borehole heat exchangers have already been constructed at several sites. Some of these are operational, while others are only being used for research purposes.

Switzerland

In 1993, in Weissbad, Switzerland, a borehole with a depth of 1,213 m was deepened to 1,600 m, this was to test the permeability of the rock. At a depth of 1,213.3 m, a cement plug was drilled into the borehole, then center pipes were installed to form a deep borehole heat exchanger (Fig. 1). When designing the exchanger, it was assumed that a temperature of approximately 15°C would be achieved in a continuous mining process, however, the actual temperature was 1.8°C lower [4].

At Weggis, the operation of the deep borehole heat exchanger has been monitored since 1994. The first phase of operation lasted from 1994 to 1996 and the borehole was underused. This was evidenced by the high temperatures of the outflowing heat carrier. The system at Weggis has proven to be reliable and robust, where it delivers thermal energy of 230 MWh per year. At present, with 40 kW of geothermal power, the unit efficiency is less than 20 $W \cdot m^{-1} \cdot K^{-1}$. The potential of this heat exchanger is estimated at around 180 kW of thermal power production [5]. The heating power is closely linked to the quality of the extracted heat energy. The lower the temperature of the extracted heat, the higher the heating power of the exchanger can be.

Germany

In the German town of Prenzlau, one geothermal borehole double was drilled in the early 1990s. Due to the poor permeability of the reservoir layer, no hot thermal water was extracted from it, but it was converted into a deep borehole heat exchanger with a depth of 2,786 m. Since 1994, with intermittent reconstructions, it has operated year-round in the load range up to 600 kW (with the help of a heat pump) [6].

A deep borehole heat exchanger with a central design was constructed on the premises of the RWTH University in the city center of Aachen. The purpose of the project was to heat the university building and conduct research. The borehole seal was made of two different cement grouts (Fig. 2). The lower part of the borehole was sealed with a grout with high thermal conductivity, while the upper part was sealed with a grout with low thermal conductivity. It was shown that with a heat carrier discharge temperature of 55°C, the heating capacity of the system would be approximately 100 kW [7].

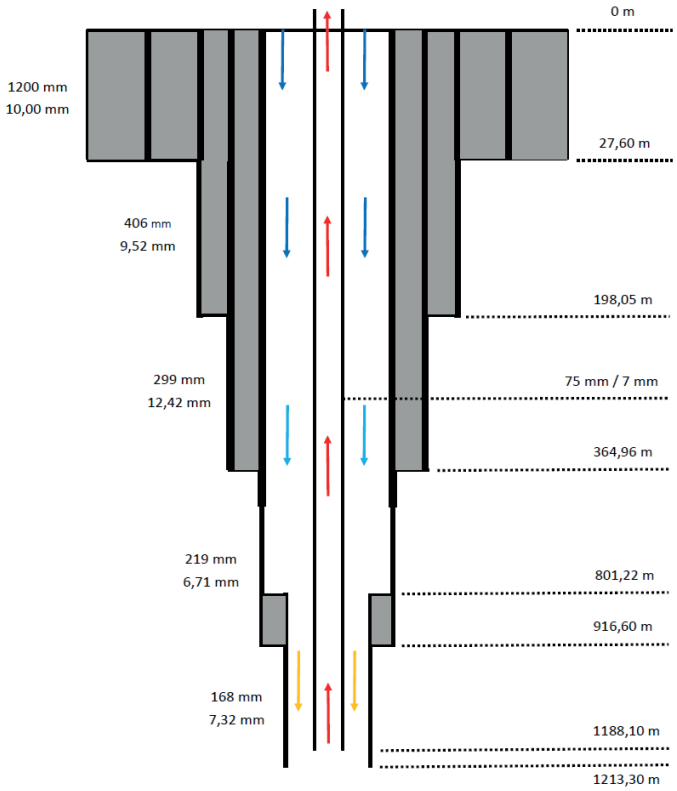

Fig. 1. Construction of a deep borehole heat exchanger with a depth of 1213 m in Weissbad, depths are given on the right, casing diameters and wall thicknesses on the left, casing – black, seal – grey (converted on the basis of [4])

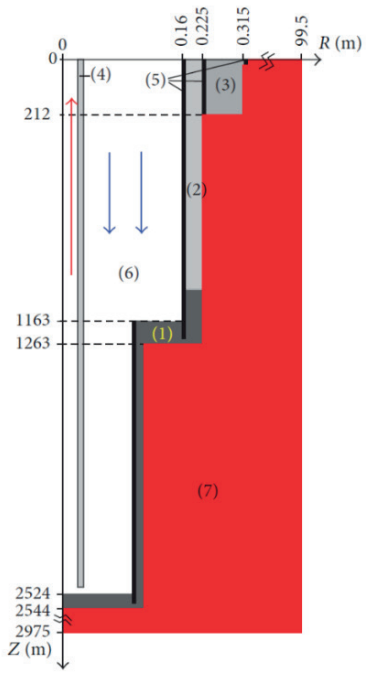

Fig. 2. Aachen heat exchanger. The 2D cylindrical grid used (radius 99.5 m and depth 2,973.5 m) with a breakdown of the different material types in the heat exchanger:
1 – high thermal conductivity cement, 2 – low thermal conductivity cement, 3 – ordinary cement, 4 – internal low thermal conductivity pipe, 5 – steel cladding pipes, 6 – water (heat carrier), 7 – surrounding rock (converted on the basis of [7])

Hungary

As part of the WeHEAT project, MS Energy Solutions Ltd. implemented Hungary's first deep borehole heat exchanger at a depth of 1800 m in the KIHA-EK-14 borehole in Kiskunhalas. A geothermal gradient of 56°C/km was calculated from the original data at the drilling of the borehole. These data were used for the first simulations, which were later made more realistic by measurements during the pilot project. Different configurations of heat carrier influent temperature to the heat exchanger (20°C, 25°C, 30°C) were tested and it was found that, with the designed borehole geometry and geological conditions, an influent temperature of 20°C was the most favorable. Simulations showed that the discharge water temperature varied between 40 and 50°C for all tested capacities. The measured and modelled temperature differences show a slight decreasing trend over time.

1.3. Geothermal heat pumps, principle of operation

A heat pump is a device that makes it possible to use distributed energy in the environment. This is only possible with the consumption of mechanical (drive) energy. The drive energy consumed by heat pumps has a higher energy utility compared to the thermal energy received in condensers [1]. Heat flow only occurs from a source that has a higher temperature to a source that has a lower temperature. If one wishes to realize the flow in the reverse direction, according to the second law of thermodynamics, drive energy must be brought in from the environment [8] (Fig. 3).

A compressor heat pump works very similarly to a refrigerator, which extracts heat from the products placed inside it and releases it outside (into the room). The unit consists of an evaporator, compressor, condenser and expansion valve (Fig. 4). The evaporator and condenser are heat exchangers [9]. In addition to this, the heat pump is equipped with various types of valves, an automation system or a working fluid reservoir.

The evaporator extracts heat from the so-called lower source, i.e. water, air, ground. Under the influence of the heat, the working medium is transformed from a liquid phase into a low-pressure, low-temperature gaseous phase. The compressor then compresses the vapor using drive energy to produce a high-temperature, high-pressure gas. In the condenser, the process of heat transfer to the heating system takes place, condensing the hot steam (transformation into a hot liquid at high pressure). The last transformation is the passage of the working medium through the expansion valve. This results in a cold liquid/steam mixture at low pressure.

In the heat pump circuit, the working medium is a fluid that receives heat from the lower source in the evaporator – at low pressure and temperature – and transfers (gives up) heat in the condenser at high temperature and pressure [3].

There are heat pumps on the market that use driving energy in the form of electricity (compressor pumps with a compressor driven by an electric motor) or high-temperature thermal energy (absorption pumps with boilers, e.g. gas-fired). Any heat pump, regardless of design, is regarded as a device that, with the help of additional energy, increases the temperature of the working medium in order to make practical use of the heat [3].

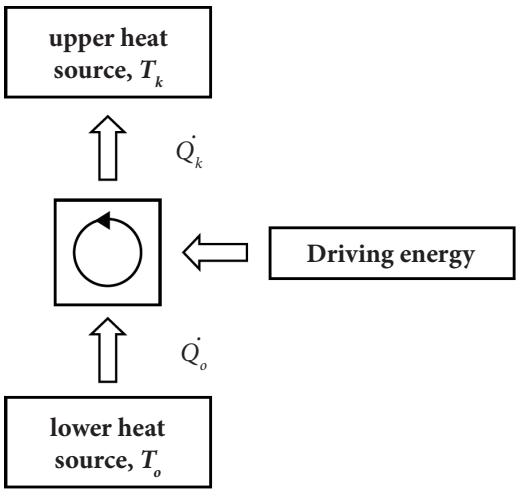

Fig. 3. Principle of energy transport in a heat pump [8]:
T_k – average flow temperature of the heat consumer, T_o – average temperature of the heat transfer medium in the evaporator, $\dot{Q}_k$ – heat flux (heating power) from the condenser to the consumer, $\dot{Q}_o$ – heat flux from the mountain to the evaporator (low-temperature heating power)

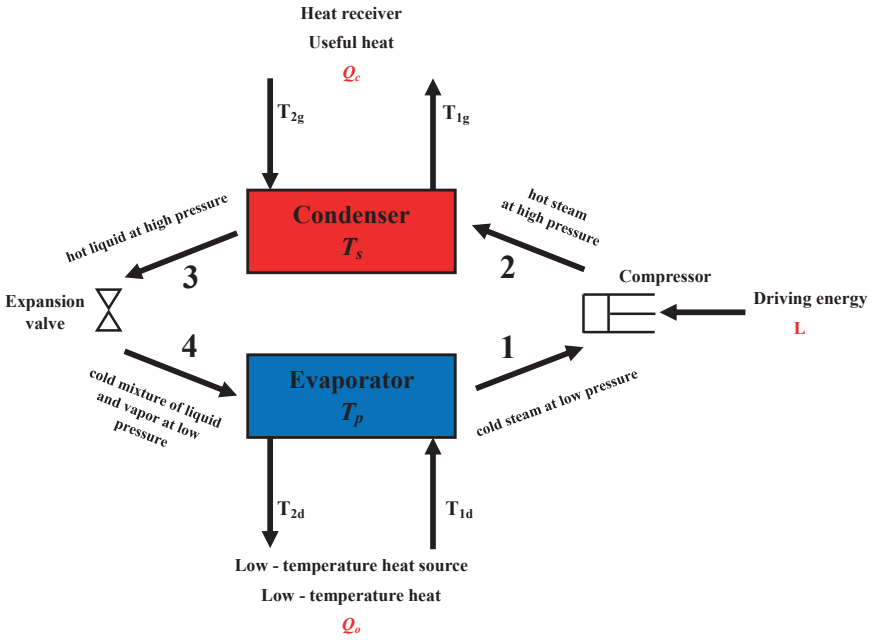

Fig. 4. Schematic diagram of the working medium circuit in a compressor heat pump [3]: T_s – condensation temperature, T_p – evaporation temperature, Q_c – heat supplied from the condenser, Q_o – heat supplied to the evaporator, L – electrical energy to drive the compressor, $T_k = (T_{2g} + T_{1g})/2$, $T_o = (T_{2d} + T_{1d})/2$, where T_{2g} – return temperature from the consumer installation (the so-called upper source), T_{1g} – supply temperature, T_{2d} – flow temperature of the borehole exchanger (the so-called lower source), T_{1d} – flow temperature of the borehole exchanger (the so-called lower source), T_{1d} – flow temperature of the evaporator (the so-called lower source). upper source), T_{1g} – supply temperature, T_{2d} – supply temperature of the borehole exchanger (so-called lower source), T_{1d} – outlet temperature from the exchanger

2. Definition of the research problem

The concept involves the design of a 3,000 m deep vertical borehole with the construction of a deep borehole heat exchanger.

2.1. Location of the project

The site of the planned borehole for the deep borehole heat exchanger is located in Krakow, Malopolska voivodship, in the area of the AGH University Campus, at Piastowska Street (Fig. 5). The plot of land on which the borehole is planned has the number 261/1. It is located at an altitude of approx. 204 m above sea level (Fig. 5).

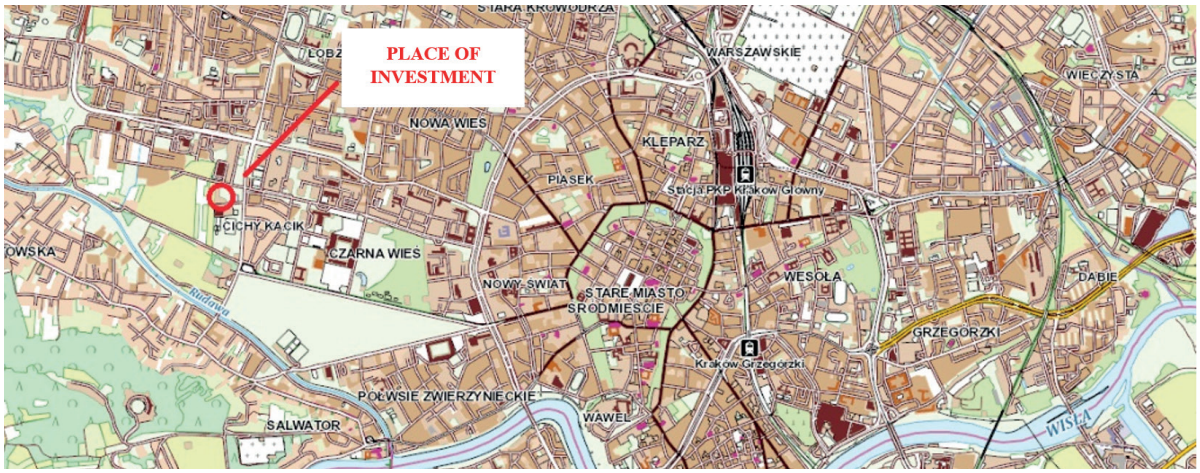

Fig. 5. Overview map No. 1 (topographic)

Source: geoportal.gov.pl

2.2. Geological structure

Krakow is located on the border of major structural units: Upper Silesian Zapadliska, Silesian-Krakow Monocline and Nida Basin, as well as the Carpathian Mountains, Pre-Carpathian Zapadliska and Carpathian Foredeep [10].

The Krakow region below ground level is built from Jurassic, Cretaceous, Miocene and Quaternary sediments (Fig. 6). As regards the Jurassic, these are shoal or rocky limestones. In the case of the Cretaceous, the marls, locally occurring on Jurassic limestones, are of low thickness. The marly clays of the Skavian strata and the clays and siltstones of the Wieliczka strata are Miocene sediments which occur almost throughout the Krakow area. The Quaternary is developed as sands and gravels with silts, water-glacial sands and loess, which occur in the north-eastern part of Krakow. The thickness of these sediments is quite variable - in places it can be up to 30 m [11]. The lithological profile with the boundary of the layers marked can be seen in Table 1 [12].

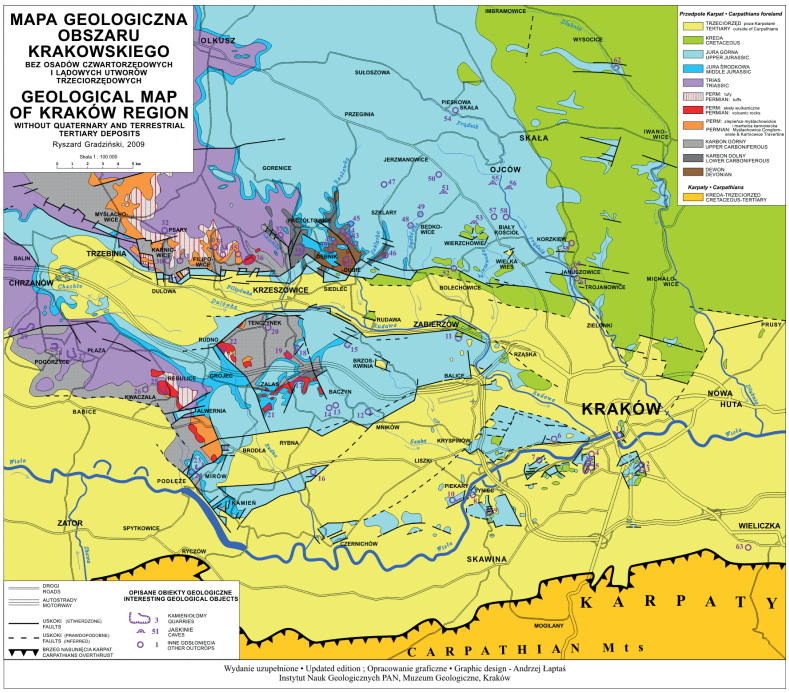

Fig. 6. Geological map of the Krakow area [13]

Table 1. Lithological profile of the analyzed borehole [12]

Layer, lithology	Top [m under surface]	Bottom [m under surface]	Thickness [m]	Density [kg/m³]	Formation type
Siltstone, shale	0	172	172	1,590	plastic
Grey altered sandstones	172	327	155	2,580	resilient
Diabase	327	423	96	2,800	resilient
Grey fine-grained sandstones	423	498	75	2,660	filtration
Shale, siltstone	498	764	266	2,260	plastic
Fine-grained sandstones	764	929	165	2,660	filtration
Dark grey shales, dark grey siltstones	929	1,160	231	2,200	plastic
Grey and dark grey limestones	1,160	1,452	292	2,620	resilient
Dolomitic limestones, dolomites 30/70	1,452	1,684	232	2,510	resilient
Beige and grey-beige dolomites	1,684	1,888	204	2,410	resilient
Grey and dark grey limestones, dolomitic limestones 10/90	1,888	2,349	461	2,509	resilient
Beige and gray-beige dolomites	2,349	3,000	651	2,410	resilient

3. Problem-solving methodology

The heat, from the deep borehole heat exchanger, will be used to cover the demand for central heating and domestic hot water. The sources must be designed as bivalent.

3.1. Design of the borehole casing

Borehole pressure and strength calculations were carried out. The pressure distribution in relation to depth (gradients) was summarized in diagram form (Fig. 7). Table 2 summarizes the values of pressures in individual lithological layers. Table 2 summarizes the values of pressure gradients in the borehole for individual layers.

Strength calculations made it possible to design the pipe columns in the borehole and, more specifically, their permissible lengths. Based on the H_{di} factor, which determines the tensile strength of the steel pipe, the lengths of the individual casing columns were selected:

- pre-column – 0–60 m;
- guidance column – 0–498 m;
- technical column I – 348–1160 m:
  - section I – 348–600 m,
  - section II – 600–900 m,
  - section III – 900–1160 m;
- technical column I – 1110–3000 m:
  - section I – 1110–1750 m,
  - section II – 1750–2350 m,
  - section III – 2350–3000 m.

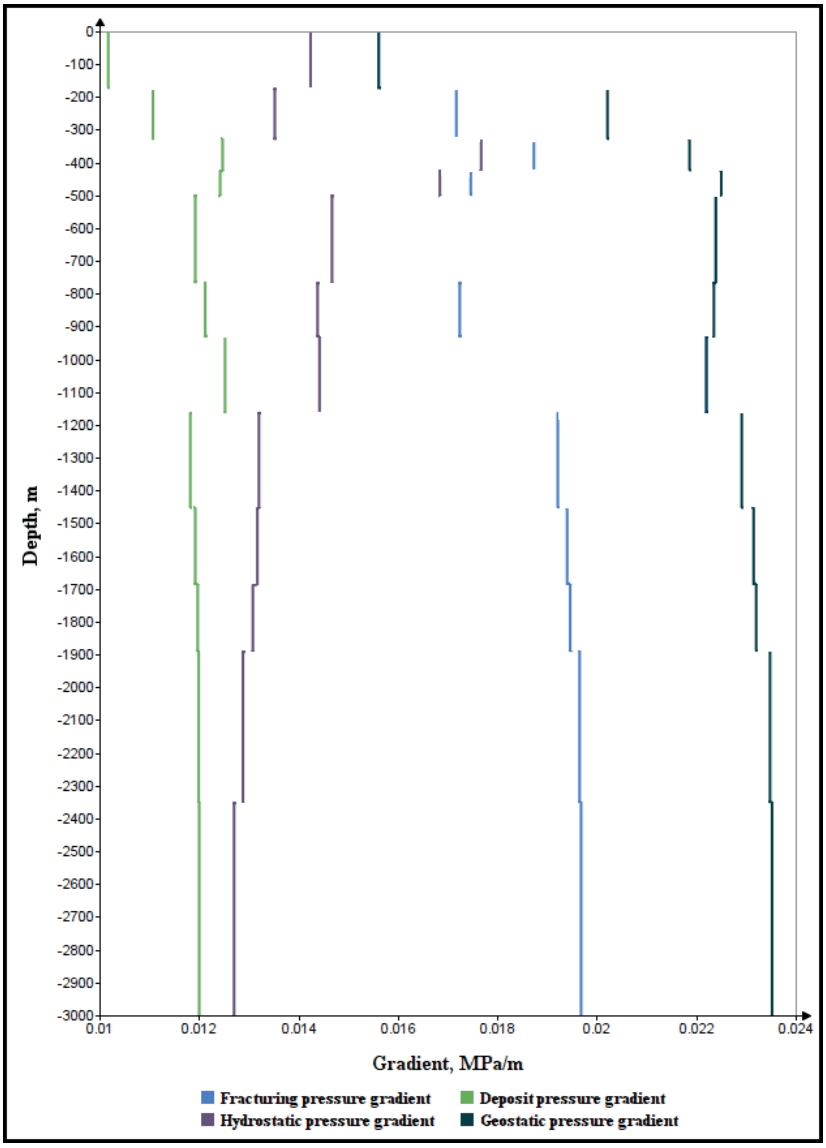

Fig. 7. Diagram of pressure gradients in a borehole

Table 2. Borehole pressures for individual layers

Layer, lithology	Top [m under surface]	Bottom [m under surface]	Thickness [m]	$p_{zł}$ [MPa]	p_g [MPa]	p_{sz} [MPa]	p_h [MPa]
Siltstone, shale	0	172	172	1,746	2,682	2,682	2,446
Grey altered sandstones	172	327	155	3,613	3,922	5,607	4,413
Diabase	327	423	96	5,266	2,636	7,915	7,466
Grey fine-grained sandstones	423	498	75	6,175	1,956	8,686	8,375
Shale, siltstone	498	764	266	9,092	5,895	17,091	11,192
Fine-grained sandstones	764	929	165	11,241	3,657	15,995	13,341
Dark grey shales, dark grey siltstones	929	1,160	231	14,500	4,984	25,732	16,700
Grey and dark grey limestones	1,160	1,452	292	17,134	7,502	27,868	19,134
Dolomitic limestones, dolomites 30/70	1,452	1,684	232	20,040	5,711	32,643	22,140
Beige and grey-beige dolomites	1,684	1,888	204	22,562	4,821	36,698	24,662
Grey and dark grey limestones, dolomitic limestones 10/90	1,888	2,349	461	28,118	11,343	46,112	30,218
Beige and gray-beige dolomites	2,349	3,000	651	35,940	15,386	58,977	38,040

Table 3. Values of borehole pressure gradients for individual layers

Layer, lithology	$G_{zł}$ [MPa]	G_g [MPa]	G_{sz} [MPa]	G_h [MPa]
Siltstone, shale	0.01015	0.01559	0.01559	0.01422
Grey altered sandstones	0.01105	0.02019	0.01715	0.01350
Diabase	0.01245	0.02184	0.01871	0.01765
Grey fine-grained sandstones	0.01240	0.02248	0.01744	0.01682
Shale, siltstone	0.01190	0.02237	0.02237	0.01465
Fine-grained sandstones	0.01210	0.02233	0.01722	0.01436
Dark grey shales, dark grey siltstones	0.01250	0.02218	0.02218	0.01440
Grey and dark grey limestones	0.01180	0.02289	0.01919	0.01318
Dolomitic limestones, dolomites 30/70	0.01190	0.02313	0.01938	0.01315
Beige and grey-beige dolomites	0.01195	0.02318	0.01944	0.01306
Grey and dark grey limestones, dolomitic limestones 10/90	0.01197	0.02346	0.01963	0.01286
Beige and gray-beige dolomites	0.01198	0.02350	0.01966	0.12680

For reasons of strength as well as cost efficiency, the individual casing columns are designed as a telescopic assembly composed of sections with different diameters and wall thicknesses. This stepped layout tailors material grade and geometry to the expected loads and hydrogeological conditions at depth, while minimizing steel use and simplifying installation.

Table 4 shows the details of the casing used for the borehole casing project, together with the diameters of the augers drilling the sections.

Figure 8 shows a diagram of how the borehole is lined up with the internal exchanger pipe: VIT 4 ½″ × 3 ½″ pipe.

Table 4. Data of casing and augers for drilling the given sections, one wall thickness is assumed for all sections of a given column

Casing pipe, OD		Steel grade	ID [m]	b [mm]	ODC [m]	D_{bit}	
[in]	[m]					[in]	[m]
$18^5/_8$	0,4731	K55	0.4510	11.05	0.5080	24	0.6096
$13^3/_8$	0,3397	J55	0.3153	12.19	0.3651	17½	0.4445
Section I, $9^5/_8$	0,2445	K55	0.2224	11.05	0.2699	12¼	0.3112
Section II, $9^5/_8$	0,2445	L80	0.2224	11.05	0.2699	12¼	0.3112
Section III, $9^5/_8$	0,2445	N80	0.2224	11.05	0.2699	12¼	0.3112
Section I, 7	0,1778	K55	0.1594	9.19	0.1945	8½	0.2159
Section II, 7	0,1778	L80	0.1594	9.19	0.1945	8½	0.2159
Section III, 7	0,1778	N90	0.1594	9.19	0.1945	8½	0.2159

Explanations: ID – inner diameter of casing pipe, b – wall of thickness, ODC – outer diameter of the connector, D_{bit} – borehole diameter, OD – outer diameter of the casing pipe

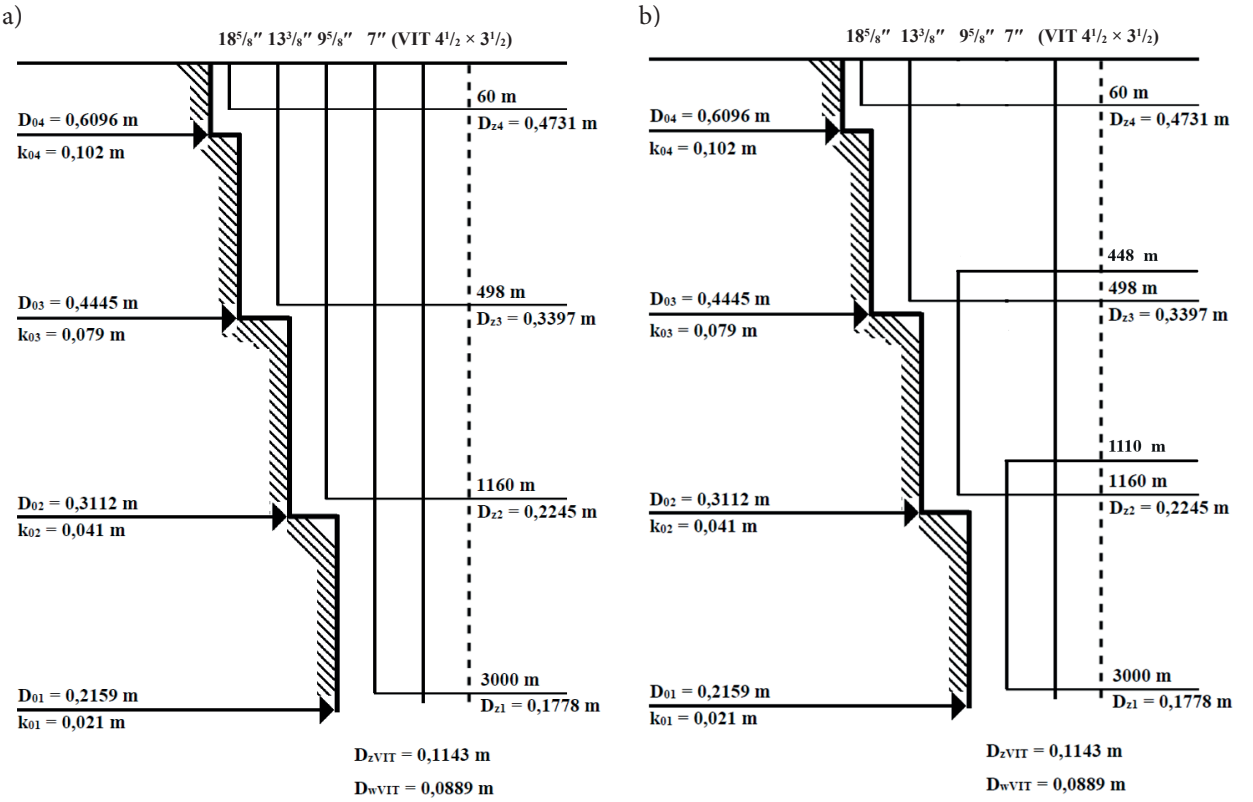

Fig. 8. Schematic of a borehole casing with VIT pipes. The design of the borehole with "overlapping" (liner) pipes can be implemented as decided at the borehole design stage: a) full casing option; b) economy option

Depending on the temperature of the injection medium, the method of cementing the cladding pipe columns can vary. Thus:

– If the temperature of the heat carrier to be injected into the GOWC is below the mean atmospheric air temperature, the entire borehole can be cemented with grout with increased thermal conductivity.
– If the temperature of the brine to be injected into the GOWC is above the mean atmospheric air temperature, the brine may additionally cool down during the initial flow phase. Therefore, up to a certain depth, thermal insulation is recommended. This can be realised by means of cement grout with reduced thermal conductivity or "overlapping" cementing and filling the inter-pipe space with nitrogen.

3.2. Deep borehole heat exchanger design

The first variant assumes the use of Vacuum Isolated Tubing (VIT). These tubes are designed to minimize heat transfer between the injected fluid, at a lower temperature (in the annular space), and the receiving fluid, at a higher temperature (flowing counterclockwise inside the column tubes). This variant assumes that the well is equipped with a column of double VIT-type tubing.

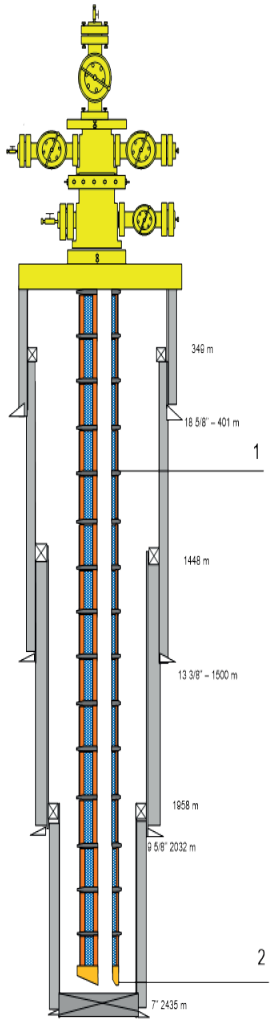

Fig. 9. Design of the Knott GT-1 well, Variant I using VIT tubing; 1 – VIT tubing 3½″ × 4½″, 2 – pipe shoe 3½″ × 4½″ [14]

The second variant involves casing two pipe columns which will be sealed at the bottom of the borehole with suitable components. Reduced-pressure nitrogen will be placed between the pipe columns as insulation to minimize heat transfer by using a vacuum pump. The sealing of the two pipe columns with the packer is shown in Figure 10.

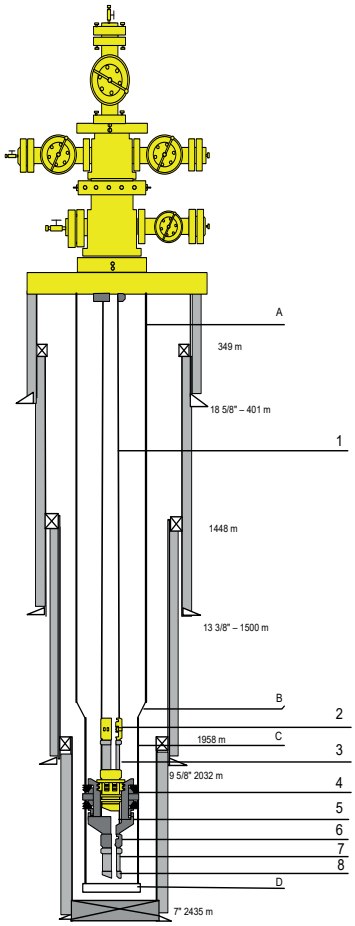

Fig. 10. Sękowa GT–1 well design, variant II using packer/sealer: A – 7″ pipes, B – 7″ coupling ×5″, C – 5″ pipes, D – 5″ open pipe shoe, 1 – 2⅞″ or 3½″ pipes, 2 – circulating sleeve, 3 – production pipe, 4 – packer, 5 – transition coupling, 6 – foundation coupling, 7 – production pipe, 8 – pipe shoe [14]

Vacuum tubes (VIT) have their origins in the oil industry, having been developed to minimize heat transfer between their interior and the annular space. They have found use in cases:

- When producing or circulating hot fluid through production tubing, e.g. in a permafrost zone, where it is undesirable to thaw the ground surrounding the well, which could cause it to lose its properties and uncontrolled subsidence of the ground around the wellhead could occur.
- When paraffin plugs and hydrates form during production of reservoir fluids and it is difficult or ineffective to use other methods that would prevent their formation.
- When hot fluids (e.g. solvents) or vapours are injected, with advanced extraction methods such as CSS (Cyclic Steam Stimulation) and SAGD (Steam Assisted Gravity Drainage), where cooling of the injected fluid is undesirable. In these meth-

ods, large amounts of energy must be expended to maximise the heating of the injected fluids, vapour, in order to transfer the elevated temperature to the in-situ reservoir fluids. The CSS method involves alternating periods of injecting superheated vapour into the reservoir and then extracting the heated oil through the same well. The SAGD method involves drilling two horizontal wells, where the horizontal part of the injection well is above the horizontal part of the production well. Steam is injected through the injection hole and the heated oil flows into the production hole.

– Where warm oil is transported along the seabed.

Variant II

This technology uses two columns of pipe that are plugged independently of each other. A packer is clipped onto the inner column which, when clipped, seals the space between the two pipe columns from the bottom of the borehole. A circulation sleeve is then opened, through which fluid is forced out of the supra-packer space using nitrogen. Once the space has been emptied of fluid, the circulation sleeve is closed and the nitrogen is drained from the space and then, using a vacuum pump, the pressure is lowered to reduce the thermal conductivity between the fluid being injected and the fluid being withdrawn from the borehole. Also important in this technology is the proper centralization of the inner column and the use of protectors made of a suitable material with low thermal conductivity.

Variant III

This technology uses two columns of pipe that are plugged independently of each other as with Variant II. Once the inner column has been collapsed, a locator at the end of the column is inserted into the PBR, ensuring a tight connection between the columns. Then, using nitrogen, the fluid between the tube columns is removed through a sleeve. Once all the fluid has been extruded from the space between the two columns, the nitrogen is released and the pressure is further reduced by using a vacuum pump. The reduction in pressure ensures a reduction in the thermal permeability of the entire insulating column. PBR – Polished Bore Receptacle, is a piece of borehole equipment into which a locator with a section of seals is inserted to ensure the tightness of the combined elements. The above solution allows the locator to move tightly in the PBR-e. In this variant, it is also important to use, among other things, plastic centralizers/protectors to avoid direct contact between the steel pipe columns and the formation of thermal bridges.

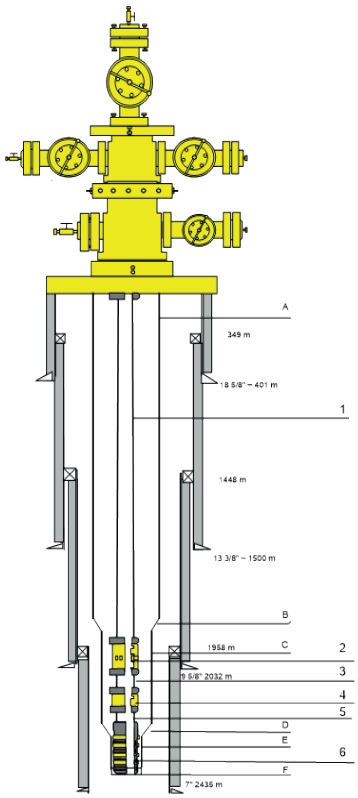

Fig. 11. Design of the Sękowa GT–1 well, Variant III using PBR: A – 7″ pipes, B – 7″ coupling × 5″, C – 5″ pipes, D – 5″ × 4,094″ ACME connector, E – PBR sealant, F – open shoe, 1 – 2⅞″ or 3½″ pipes, 2 – circulation sleeve, 3 – production pipe, 4 – foundation connector, 5 – production pipe, 6 – locator/stinger [14]

4. Summary

The results of drill stem test of the reservoir at various intervals in the borehole have ruled out the possibility of developing it as a classic geothermal borehole. Unfortunately, the requirements for the borehole to be used as a geothermal borehole were not met.

On the basis of the tests and analyses carried out, it can be concluded that the temperature in the designated measurement intervals stabilizes to certain values during both the plugging and pulling out of the loggers, so the measurement methodology employed can be described as correct. However, three measurements taken at longer intervals indicated a lack of complete stabilization, following a disturbance of the natural temperature during the drilling process. This can be concluded from the high accuracy of the thermometers used.

Variant III was chosen to proceed further for technical and economic reasons. The biggest disadvantage of Option I was its high price, due to the cost of purchasing

and supplying vacuum tubes (VIT). Option II required a longer operation time – an additional walk to get the pacer on the tube. Variant III was the most financially advantageous, moreover, the length of the PBR and the locator allows some length tolerance in the selection of the packer and possibly easy replacement.

A large number of deep wells and boreholes have been developed for the oil industry in Poland, and they are not infrequently located close to urbanized areas. If even a small proportion of these were used to harness the heat of the rock mass, the amount of geothermal energy extracted could be increased. Counting only the 1980s, more than 4,500 boreholes with a depth of more than 500 m were drilled in Poland, according to Table 5, which shows the number of boreholes drilled in Poland since 1980, according to the Polish Geological Institute. In addition, after analyzing the map presented in Figure 12, it may be noted that high rock mass temperatures occur, inter alia, in the vicinity of Poznań and Gorzów Wielkopolski, where intensive work on hydrocarbon exploration and production was carried out for many years, so there are many boreholes in those areas which are nearing the end of their exploitation or are already destined for decommissioning. Therefore, the topic of adapting deep boreholes and boreholes for borehole heat exchangers should be developed further.

Table 5. Number of boreholes drilled in Poland since 1980 according to the National Geological Institute [1]

No.	Maximum borehole depth [m]	Number of wells drilled in Poland since 1980
1	500	4,563
2	100	3,676
3	1,500	2,575
4	200	1,721
5	2,500	1,228
6	3,000	826
7	3,500	385
8	4,000	188
9	3,500	84
10	5,000	38
11	5,500	13

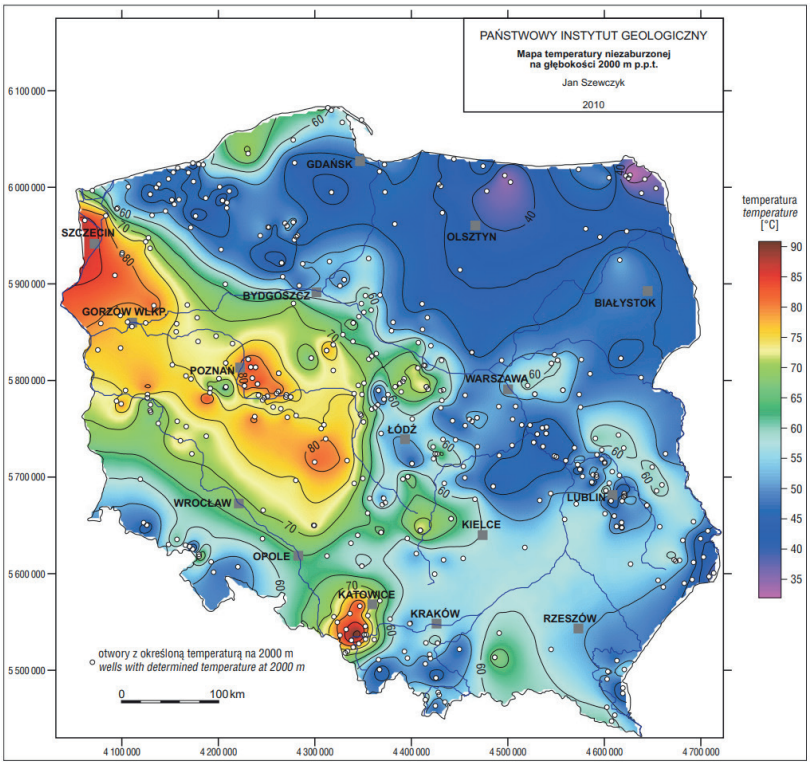

Fig. 12. Poland's geothermal potential at a depth of 2,000 m [3]

The third variant assumes an arrangement that is similar to variant II with the difference that a PBR and locator would be used instead of the sealing elements which are the packer in variant II [14].

5. Conclusions

– The low thermal conductivity of the inner column of the exchanger is very important for the thermal isolation of the heat transfer medium flowing into it, from the medium flowing in the annular space – especially the closer you get to the surface, because of the increasing radial temperature gradient.
– Each well should be approached individually, carefully analyzing the geological conditions of the well, the thermal parameters of the strata and the location of the future use of the deep borehole heat exchanger. The three proposed variants for the construction of a deep borehole heat exchanger will allow the developer to select one on the basis of the chosen criteria(s).

Author contributions: Conceptualization T.S., formal analysis, methodology, writing–review and editing, writing–original draft preparation, and investigation, R.K.; supervision T.S., validation, project administration, A.S. All of the authors have read and agreed to the published version of the manuscript.

Funding: This research received no external funding.

Conflicts of Interest: The authors of this paper declares no conflicts of interest.

References

[1] Gonet A. (red.): *Metodyka identyfikacji potencjału cieplnego górotworu wraz z technologią wykonywania i eksploatacji otworowych wymienników ciepła*. Wydawnictwa AGH, Kraków 2011.
[2] Śliwa T., Wolan M., Mazur C., Wójtowicz T.: *Adaptacja istniejących i zlikwidowanych odwiertów na głębokie otworowe wymienniki ciepła. Technologia wykonania końcowego wyposażenia otworu do pozyskiwania ciepła z górotworu*. In: A. Kasztelewicz (red.), *VII Ogólnopolski Kongres Geotermalny 28–30 IX 2021* [online]. Polskie Stowarzyszenie Geotermiczne, Kraków 2021, pp. 176–178.
[3] Śliwa T. (red.): *Zintegrowany system otworowych wymienników ciepła i kolektorów słonecznych*. Wydawnictwa AGH, Kraków 2012.
[4] Kohl T., Salton M., Rybach L.: *Data analysis of the Deep Borehole Heat Exchanger plant Weissbad (Switzerland)*. In: *Proceeding World Geothermal Congress, May 28 – June 10, 2000, Kyushu–Tohoku, Japan*, 2000, pp. 3459–3464.
[5] Kaltschmitt M., Huenges E., Wolff H.: *Energie aus Erdwärme: Geologie, Technik und Energiewirtschaft*. Verlag für Grundstoffindustrie, Stuttgart 1999.
[6] Doelling R.J., Schulte I.: *Deep Groundsourced Heat Exchanger with Coaxial Pipe, Closed Water Circuit – Improvement Proposals in Project Development and Technical Pipe Conception Beitrag*. In: *Der Geothermiekongress*. Bochum 2009.
[7] Dijkschoorn A., Wagner R.: *Performance simulations for a deep borehole heat exchanger in Aachen*. In: *GGE Published Workshop on New and Classical Applications of Heat Flow Studies*. Aachen 2004.
[8] Bohdal T., Charun H., Sikora M.: *Wybrane aspekty prawno-techniczne i ekologiczne stosowania sprężarkowych pomp ciepła*. Rocznik Ochrona Środowiska, 17, 2015, pp. 461–484.
[9] Adamczewski A.: *Budowa sprężarkowej pompy ciepła – instsani.pl*, 2022. https://instsani.pl/ [7.08.2022].
[10] Rutkowski J.: *Budowa geologiczna regionu Krakowa*. Przegląd Geologiczny, 37, 6, 1989, pp. 302–308.
[11] Płoskonka J.: *Wstępna opinia geologiczno-inżynierska dla projektu 3 linii premetra w Krakowie*. PGG "Geoprojekt" Sp. z o.o. w Krakowie, Kraków 2009.
[12] Płaza K.: *Projekt głębokiego otworowego wymiennika ciepła* [diploma project thesis]. AGH University, Kraków 2021.
[13] Gradziński R.: *Mapa geologiczna obszaru krakowskiego bez osadów czwartorzędowych i lądowych utworów trzeciorzędowych*, Instytut Nauk Geologicznych PAN, Kraków 2009.
[14] Wolan M., Śliwa T., Dziadzio P.: *Wyposażenie wgłębne głębokiego otworowego wymiennika ciepła do pozyskania ciepła Ziemi*. Wiadomości Naftowe i Gazownicze, 26, 1, 2023, pp. 4–13.

Journal of Geotechnology and Energy | vol. 42 | no. 2 | 2025 | pp. 29–37

https://doi.org/10.7494/jge.2025.42.2.7116

ARTICLE

Jacek Blicharski

AGH University of Krakow, Faculty of Drilling, Oil and Gas, Poland
ORCID: 0000-0003-2082-6590
e-mail: jblich@agh.edu.pl

Izabela Dybaś

Independent Researcher
Polska Spółka Gazownictwa sp. z o.o.
ORCID: 0009-0005-0275-031X
e-mail: izabela.dybas@psgaz.pl

THE IMPACT OF RESERVOIR PARAMETERS AND WELL CONSTRUCTION ON GAS WELL PRODUCTIVITY

Date of submission:
27.03.2025

Date of acceptance:
10.04.2025

Date of publication:
30.06.2025

https://journals.agh.edu.pl/jge

Abstract: The aim of this paper was to present the influence of selected reservoir parameters and well construction on the productivity of a gas well, using the example of a natural gas reservoir with high nitrogen content. Data from an exemplary well were used to carry out a variant assessment of the productivity of wells at different stages of reservoir exploitation, taking into account single- and two-phase gas-condensate mist flow in the well. The reservoir development process is briefly described at the beginning. Subsequently, the issues of gas inflow to the well, gas flow in the well and nodal analysis were discussed. The last part of the paper focuses on the variant assessment of the productivity at different stages of reservoir exploitation using a computational algorithm for single-phase and two-phase gas-condensate mist flow in the well.

Keywords: nitrogen gas reservoir, gas well productivity, deliverability, inflow performance relationship, vertical lift performance, nodal analysis

1. Introduction

Natural gas is a raw material playing a significant role in the energy and chemical industries. A discovered natural gas reservoir is characterized by the following parameters: initial pressure, reservoir thickness, porosity, permeability, reservoir temperature and the composition of the reservoir fluid. Based on these criteria which define the reservoir, it is possible to determine whether there are balance resources and then under economic and technical conditions, industrial resources [1]. Once industrial resources of natural gas are confirmed, the hydrocarbon reservoir is developed. The well or wells providing access to the reservoir are tested with a tubular reservoir sampler. Subsequently, the well is secured both internally and at the surface. A production string is lowered into the production casing, enabling the flow of reservoir fluid from the bottom of the well to the surface while protecting the production casing from the effects of high reservoir pressure and the components of gas that contribute to corrosion and damage to the inner walls of the pipes. A production tree is attached to the production string, which serves as the surface security of the well and simultaneously allows connection to a system designed for receiving and treating the reservoir fluid. Before the commencement of reservoir exploitation, each well is tested to determine its production capacity [2].

The productivity of a gas well is the maximum amount of gas that can be extracted from the reservoir using a well in a given time, most often expressed in units of Scm/s (m^3 of gas at standard conditions per second). It depends on the geological parameters of the reservoir, in particular on the reservoir pressure, the permeability and thickness of the reservoir, as well as on the well parameters, such as the diameter of the production pipes used to access the reservoir. The efficiency of the well also depends on the composition of the reservoir fluid itself, including its viscosity and density, which affects its flow through the rock medium [3].

There are two fields of high nitrogenous natural gas in Poland. These reservoirs are called Sulęcin and Cychry. One of them, Cychry, is localized in the Polish Lowland. The gas is composed of over 90% nitrogen and this reservoir is accessed by two wells which have a similar construction and depth [4].

In order to determine optimal extraction, obtain information on reservoir parameters and determine the production zones of a given reservoir, hydrodynamic tests are performed, consisting of the creation of a state of non-equilibrium in the well while simultaneously measuring the reaction of the reservoir to the pressure disturbance that occurs in it. The reaction of the reservoir is recorded by measuring pressure changes over time [5].

2. Methodology

2.1. Gas inflow to the well

The gas inflow to the well can be described by the reservoir performance curve, abbreviated as the "IPR curve – Inflow Performance Relationship", which is a function of the relationship between the pressure at the bottom of the well and the flow rate. It is determined based on the gas inflow equation (1) named two-term formula [6]:

$$p_{bh} = \sqrt{p_r^2 - \frac{\mu \cdot z \cdot p_{sc} \cdot T}{\pi \cdot k \cdot h \cdot T_{sc}} \cdot \left(\ln \frac{r_e}{r_w} - \frac{3}{4} + S_m \right) \cdot q} \cdot \sqrt{- \frac{\mu \cdot z \cdot p_{sc} \cdot T}{\pi \cdot k \cdot h \cdot T_{sc}} \cdot D_t \cdot q^2} \tag{1}$$

where:

p_{bh} – bottomhole pressure [Pa],
p_r – average reservoir pressure [Pa],
q – gas flow rate [Scm/s],
k – reservoir permeability [m^2],
μ – gas viscosity [Pa·s],
z – gas compressibility factor [–],
p_{sc} – pressure at standard conditions [Pa],
T – reservoir temperature [K],
T_{sc} – temperature at standard conditions [K],
r_e – outer boundary radius [m],
r_w – wellbore radius [m],
S_m – mechanical skin factor [–],
h – reservoir thickness [m],
D_t – turbulence coefficient [s/m^3].

In a simplified form, this formula appears as follows:

$$p_{bh} = \sqrt{p_r^2 - a \cdot q - b \cdot q^2} \tag{2}$$

where:

$$a = \frac{\mu \cdot z \cdot p_{sc} \cdot T}{\pi \cdot k \cdot h \cdot T_{sc}} \cdot \left(\ln \frac{r_e}{r_w} - \frac{3}{4} + S_m \right)$$

$$b = \frac{\mu \cdot z \cdot p_{sc} \cdot T}{\pi \cdot k \cdot h \cdot T_{sc}} \cdot D_t$$

Figure 1 shows well inflow performance curves for different values of the product of permeability and reservoir thickness.

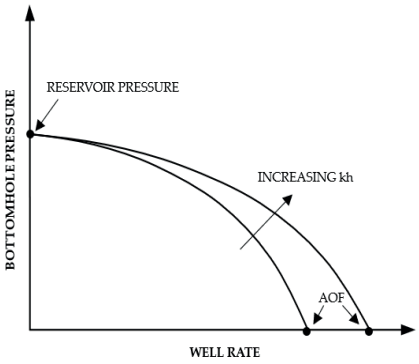

Fig. 1. Well inflow performance curves [7]

The analysis of Figure 1 shows that for zero well rate, the dynamic bottomhole pressure is equal to the average reservoir pressure. With the decrease of the bottomhole pressure the well rate increases until the bottomhole pressure reaches a value equal to atmospheric pressure, then the well rate takes on a maximum value, i.e. the potential well deliverability called "AOF", which can also be determined as a positive root of the equation of the two-term formula (1) [7]:

$$AOF = \frac{-a + \sqrt{a^2 + 4 \cdot b \cdot (p_r^2 - p_{sc}^2)}}{2 \cdot b} \tag{3}$$

From the equation (2) describing the IPR curve, it can be concluded that the slope of this curve is inversely proportional to the product of the thickness (h) and the permeability of the reservoir (k). With the increase of the product kh, the IPR curve becomes flatter.

2.2. Tubing-flow performance

The well flow rate in a well refers to the pressure drop as a function of the gas flow rate in the well. It depends on the well configuration and the properties of the transported fluid. For a single-phase gas flow in a well with constant parameters, i.e.: cross-section area, temperature, compressibility coefficient and friction, the tubing performance equation has the form [6]:

$$p_{bh} = \sqrt{p_{wh}^2 \cdot e^{\frac{2 \cdot g \cdot H}{z \cdot R \cdot T}} + \frac{8 \cdot \lambda \cdot p_{sc}^2 \cdot z^2 \cdot T^2 \cdot \left(e^{\frac{2 \cdot g \cdot H}{z \cdot R \cdot T}} - 1\right) \cdot q^2}{\pi^2 \cdot T_{sc}^2 \cdot D^5 \cdot g}} \tag{4}$$

where:

p_{wh} – wellhead pressure [Pa],
g – gravitational constant [m/s^2],
H – wellbore depth [m],
R – individual gas constant [J/kg·K],
λ – friction factor [–],
D – tubing diameter [m].

Equation (4) consists of two parts: I static – expresses the pressure of the gas column in the well and II dynamic – determines the pressure loss due to overcoming the gas flow resistance in the well.

Gas well streams can contain some liquid condensate which is usually dispersed in the gas in the form of mist. The flowing mixture of gas and condensate can be treated as a pseudo-homogeneous fluid with corresponding properties of the single phase recombined hydrocarbon fluid, i.e. the fluid obtained from recombining the well stream gas and liquid in the same proportion as they are produced. This implies that the flow behavior of a gas-condensate mixture in a wellbore can be described using single-phase flow models, as long as appropriate adjustments and modifications are made to account for the properties of the pseudo-homogeneous fluid.

In the case of two-phase gas-condensate mist flow, the equation is as follows [7]:

$$p_{bh} = \sqrt{p_{wh}^2 \cdot e^{\frac{2 \cdot g \cdot M_g \cdot H}{z_g \cdot R_u \cdot T}} + \frac{8 \cdot \lambda \cdot R_u \cdot p_{sc}^2 \cdot z^2 \cdot T^2}{M_g^2 \cdot \pi^2 \cdot T_n^2 \cdot D^5 \cdot g} \cdot \sqrt{\left(e^{\frac{2 \cdot g \cdot M_g \cdot H}{z_g \cdot R_u \cdot T}} - 1\right) \cdot \left(\rho_n \cdot q \cdot \left(1 + \frac{R_{VLG} \cdot \rho_L}{\rho_n}\right)\right)^2}} \tag{5}$$

where:

M_g – molecular mass of recombined gas [kg/kmol],
z_g – compressibility factor of recombined gas [–],
R_{VLG} – volumetric condensate/gas ratio (q_L/q_{sc}),
ρ_n – gas density at standard condition [kg/m^3],
R_u – gas constant [8314 joule/kmol·K],
ρ_L – condensate density [kg/m^3].

Figure 2 shows the well performance curves (VLP) for two different values of tubing diameters.

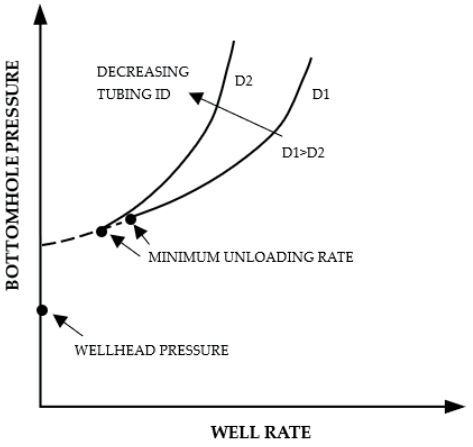

Fig. 2. Tubing flow performance [7]

Figure 2 shows VLP curves, depending on the bottomhole operating pressure from the well deliverability for different well tubing diameters at the assumed constant wellhead pressure. With the increase in the flow rate, the bottomhole operating pressure also increases and the curves deflect upwards, which is caused by the increasing flow resistance. The smaller the diameter of the tubing, the greater the flow resistance.

2.3. Nodal analysis

To determine the flow rate, nodal analysis is used, i.e. solving the system of equations for gas inflow to the well (1) and the well tubing performance equation (4) or (5). This solution can also be obtained graphically by intersecting the well performance curve (VLP) and the inflow performance curve (IPR) on a graph of p_{bh} versus q. The point at which these curves intersect determines the well deliverability, which is illustrated in Figure 3.

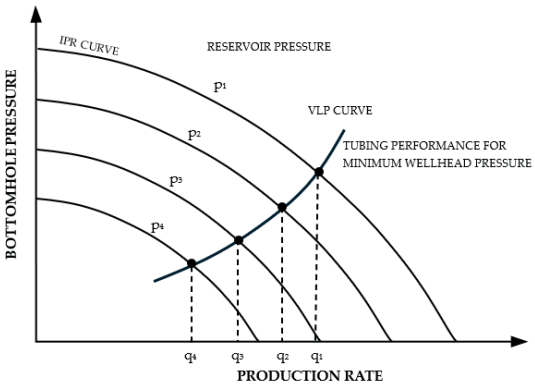

Fig. 3. Graphical determination of well deliverability using nodal analysis [7]

Figure 3 shows several IPR curves for different reservoir pressures and one VLP curve for the given wellhead pressure. These curves define several intersection points that determine the change in well performance with decreasing reservoir pressure and therefore the decrease in well production rates.

3. Calculations

Nodal analysis was used to perform variant assessment of the productivity of the well. First, calculations were made for IPR curves at three different reservoir pressures 55.13 MPa (initial reservoir pressure), 40 MPa, 30 MPa and three different reservoir permeabilities 16.2 mD, 12.1 mD, 8.1 mD. Having assumed the coefficients "a" and "b" of the two-term formula, their values were corrected due to the change in gas properties with pressure and the change in phase permeability. Permeability was reduced because with the decrease in pressure in the gas-condensate reservoir, condensate is deposited in the reservoir pores, which results in a decrease in the effective reservoir permeability.

In the next stage of calculations, VLP well performance curves were constructed for different wellhead pressures 30 MPa, 20 MPa and 12 MPa and two tubing diameters 2 7/8″ and 3 1/2″.

A multi-variant analysis was conducted to assess gas well productivity. This analysis allows for the evaluation of the impact of the a.m. parameters on the well deliverability.

The Soave–Redlich–Kwong equation was used to calculate the gas compressibility factor "Z", while the gas viscosity was determined using the Lee–Gonzalez correlation.

3.1. Data and calculation assumptions

The calculations were based on the assumed input data collected in Tables 1 and 2.

Table 1 . Composition and parameters of gas

Composition	Symbol	Molecular vol. [%]	Critical pressure [MPa]	Critical temperature [K]	Molecular mass [kg/kmol]	Acentric coefficient [–]
Methane	CH_4	5.174	4.641	190.55	16.042	0.008
Ethane	C_2H_6	1.290	4.913	305.50	30.068	0.980
Propane	C_3H_8	0.951	4.264	369.80	369.8	0.152
nButane	n-C_4H_{10}	0.292	3.796	425.17	425.17	0.193
iButane	i-C_4H_{10}	0.120	3.647	408.14	408.14	0.176
nPentane	n-C_5H_{12}	0.202	3.374	469.78	469.78	0.251
iPentane	i-C_5H_{12}	0.200	3.333	462.96	462.96	0.197
Hexane	C_6H_{14}	0.178	3.031	507.86	507.86	0.296
Azote	N_2	90.868	3.396	126.25	126.25	0.040
Carbon dioxide	CO_2	0.555	7.382	304.19	304.19	0.225
Hydrogen sulfide	H_2S	0.170	8.940	373.20	373.20	0.081

Table 2. Parameters of the well and gas properties

Parameter	Value
Depth [m]	3,333
Initial reservoir temperature [°C]	111.3
Initial reservoir pressure [MPa]	55.13
Rock permeability [mD]	16.15
Tubing diameter [in]	2 7/8
Roughness of tubing [mm]	0.015
Thickness of the reservoir [m]	30
Condensate exponent [l/m^3]	0.089
Condensate density [g/cm^3]	0.7289
Condensate density under normal conditions [kg/m^3]	1.411
Coefficient "a" of two-term formula [MPa^2/(*Scm*/min)]	0.561236295
Coefficient "b" of two-term formula [MPa^2/(*Scm*/min)^2]	$7.90858 \cdot 10^{-5}$
Pseudo-reduced temperature [K]	174.339
Pseudo-reduced pressure [MPa]	4.091
Molecular mass of gas [kg/kmol]	31.571
Gas compressibility factor "Z" at initial conditions	1.3938
Gas viscosity at initial conditions [Pa · s]	$5.296 \cdot 10^{-5}$

4. Results

As a result of the variant calculations conducted for the well, gas flow rates were determined and are presented in Tables 3–7. The constructed VLP curves are shown in Figures 4–8 and the graphical solution of the nodal analysis for each variant is also presented in these figures. The intersection points indicate the target gas well productivity for the considered variants I–V. The individual variants differed in terms of the adopted reservoir pressures, wellhead pressures, reservoir permeabilities and tubing diameters.

The values for the variants are presented in Tables 3–7.

Variant I – single-phase gas flow

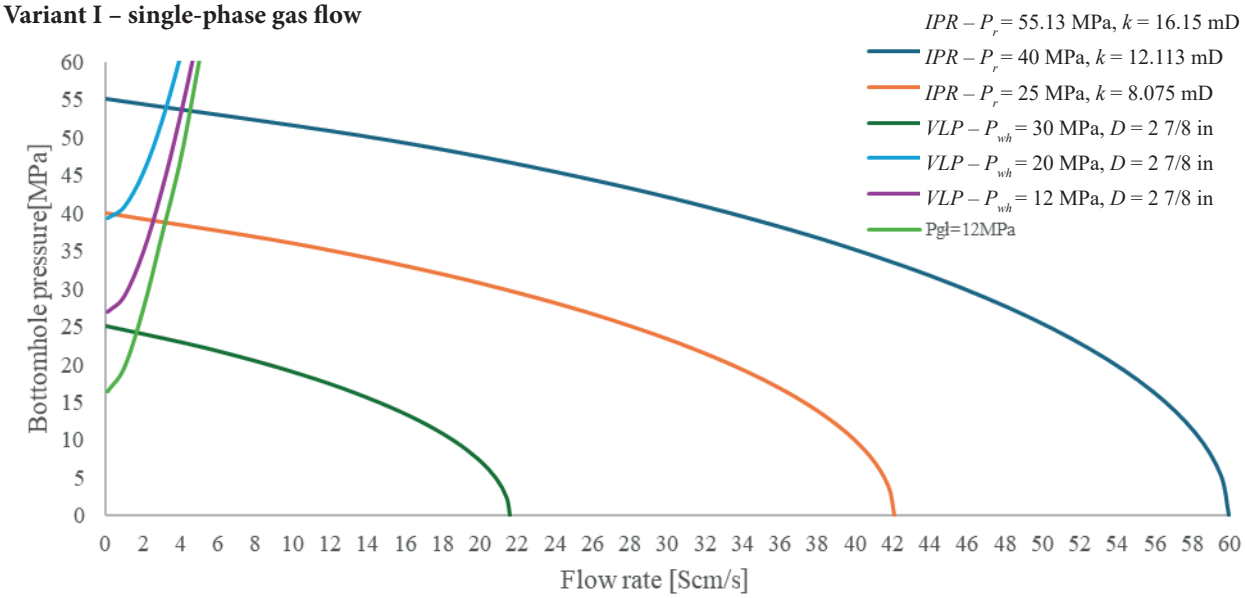

Fig. 4. IPR and VLP curves in variant I

Table 3. Well deliverability determined from the nodal analysis (variant I)

P_r [MPa]	P_{wh} [MPa]	*D* [in]	*k* [mD]	*q* [Scm/s]
55.13	30	2 7/8	16.15	**3.1**
55.13	20	2 7/8	16.15	**4**
55.13	12	2 7/8	16.15	**4.4**
40	30	2 7/8	12.113	**0.4**
40	20	2 7/8	12.113	**2.7**
40	12	2 7/8	12.113	**3.1**
25	12	2 7/8	8.075	1.8

Variant II – single-phase gas flow

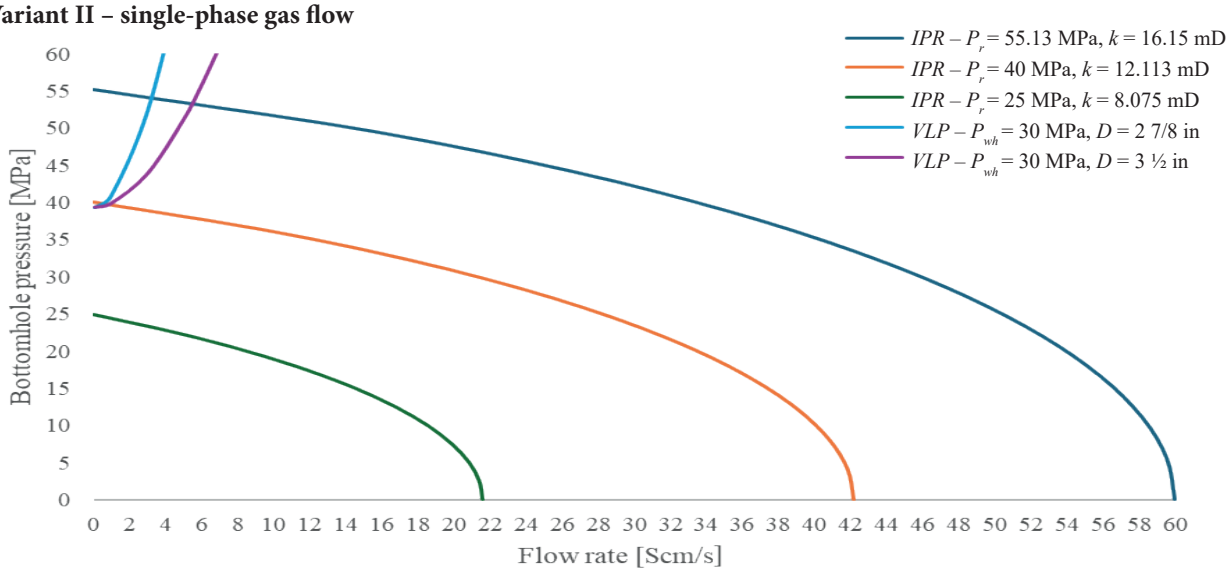

Fig. 5. IPR and VLP curves in variant II

Table 4. Well deliverability determined from the nodal analysis (variant II)

P_r [MPa]	P_{wh} [MPa]	D [in]	k [mD]	q [Scm/s]
55.13	30	2 7/8	16.15	**3.2**
55.13	30	3 1/2	16.15	**5.4**
40	30	2 7/8	12.113	**0.6**
40	30	3 1/2	12.113	**1**

Variant III – single-phase gas flow

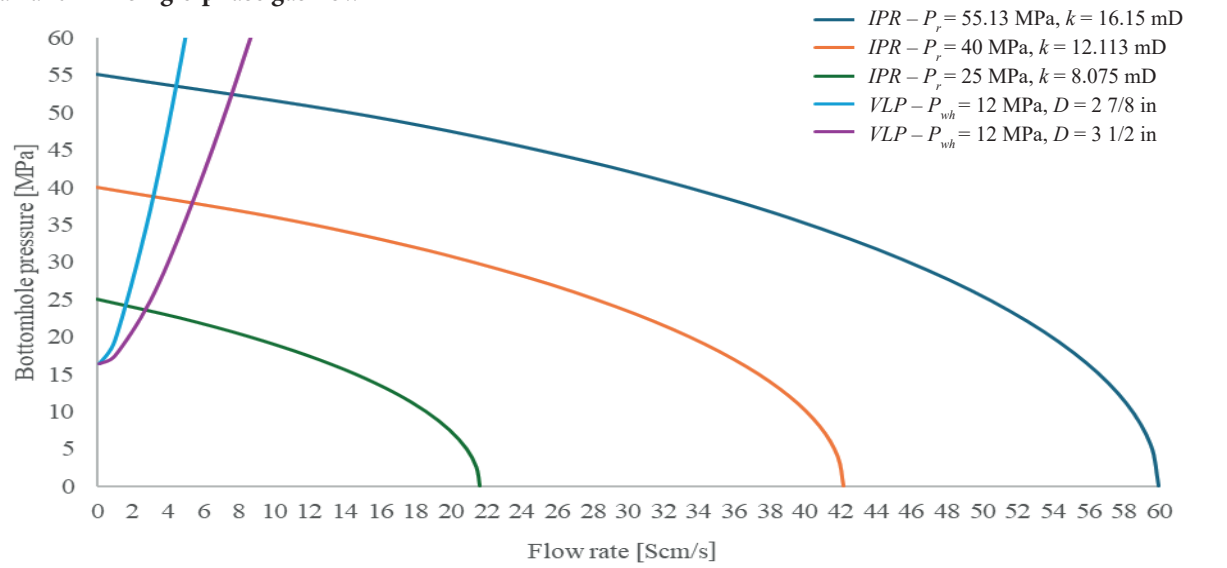

Fig. 6. IPR and VLP curves in variant III

Table 5. Well deliverability determined from the nodal analysis (variant III)

P_r [MPa]	P_{wh} [MPa]	D [in]	k [mD]	q [Scm/s]
55.13	12	2 7/8	16.15	**4.4**
55.13	12	3 1/2	16.15	**7.7**
40	12	2 7/8	12.113	**3.1**
40	12	3 1/2	12.113	**5.3**
25	12	2 7/8	8.075	**1.6**
25	12	3 1/2	8.075	2.8

Variant IV – two-phase gas-condensate mist flow

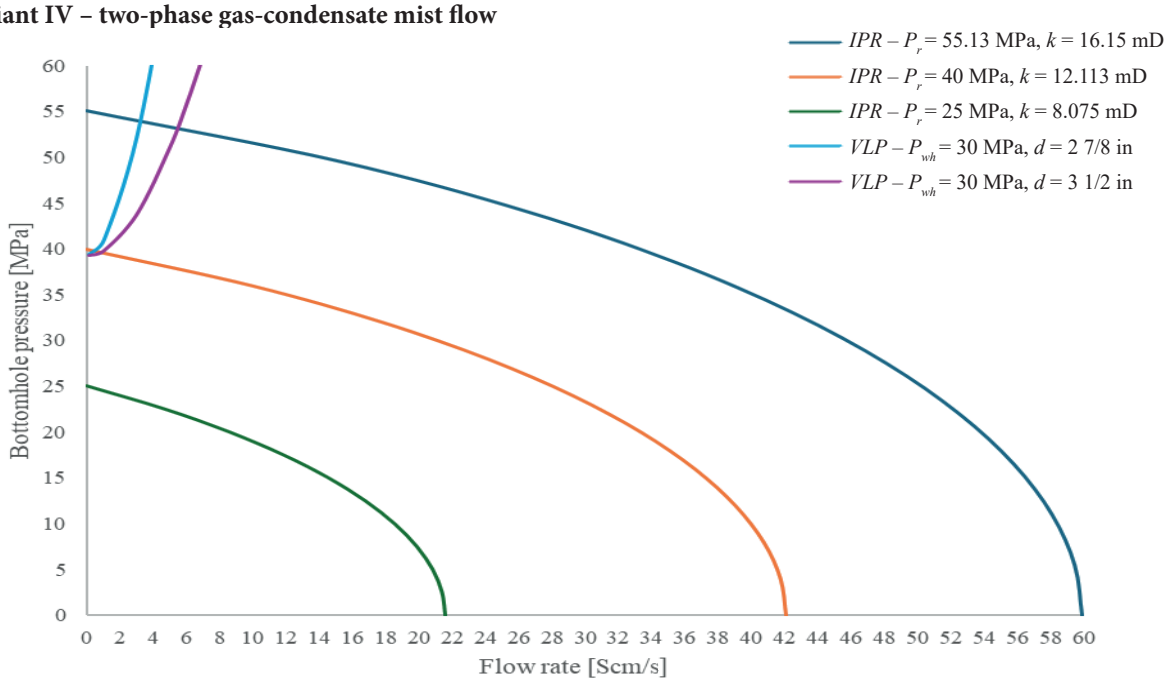

Fig. 7. IPR and VLP curves in variant IV

Table 6. Well deliverability determined from the nodal analysis (variant IV)

P_r [MPa]	P_{wh} [MPa]	D [in]	k [mD]	q [Scm/s]
55.13	30	2 7/8	16.15	**3**
55.13	30	3 1/2	16.15	**5.2**
40	30	2 7/8	12.113	**0.4**
40	30	3 1/2	12.113	**0.7**

Variant V – two-phase gas-condensate mist flow

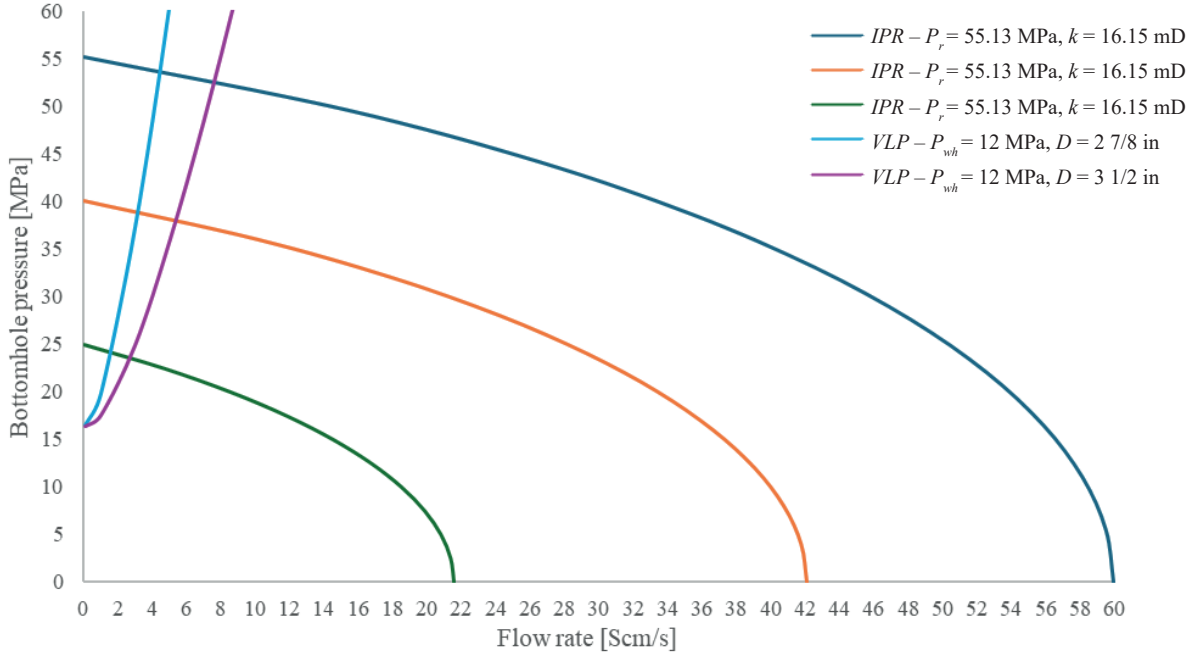

Fig. 8. IPR and VLP curves in variant V

Table 7. Well deliverability determined from the nodal analysis (variant V)

P_r [MPa]	P_{wh} [MPa]	D [in]	k [mD]	q [Scm/s]
55.13	12	2 7/8	16.15	**4.2**
55.13	12	3 1/2	16.15	**7.3**
40	12	2 7/8	12.113	**3**
40	12	3 1/2	12.113	**5.1**
25	12	2 7/8	8.075	**1.5**
25	12	3 1/2	8.075	**2.6**

4.1. Analysis of the results

In variant I, the well deliverability was determined at the formation pressures of 55.13 MPa (initial reservoir pressure), 40 MPa and 25 MPa, and wellhead pressures of 30 MPa, 20 MPa and 12 MPa, with a constant diameter of the production pipes of 2 7/8 in. The highest well deliverability was obtained at the initial formation pressure and the lowest wellhead pressure (12 MPa), which was 4.4 Scm/s. The calculations show that well deliverability decreases with a decrease in reservoir pressure and is lower at higher wellhead pressures.

In variants II and III, the influence of the diameter of the production tubes on the productivity of the well was analyzed. Higher well deliverability was obtained for a larger diameter of the production tubes and lower values of the wellhead pressure. The highest well deliverability was obtained in variant 3 for the diameter of the production tubes 3 1/2 in at the initial pressure and the wellhead pressure of 12 MPa and it amounted to 7.7 Scm/s.

Variants IV and V are modifications of variants II and III. In these variants, two-phase gas and condensate flow in the well was considered. The obtained results indicate a slight decrease in the well deliverability in both variants, i.e. IV and V, compared to variants II and III, which is caused by a greater pressure loss on the fluid flow in the well. In turn, this is caused by the increase in the gas column pressure and greater gas flow resistance with the condensate. The highest well deliverability value was obtained in variant V at a formation pressure of 55.13 MPa and a wellhead pressure of 12 MPa. In these conditions, the efficiency reached 7.3 Scm/s and was 5.2% lower compared to variant III. In variant IV, at an initial pressure of 55.13 MPa, the maximum well deliverability of 5.2 Scm/s was achieved, which was 3.7% lower compared to variant II.

5. Conclusions

The analysis conducted showed that the product of permeability and reservoir thickness has a significant impact on the productivity of the well; higher permeability enables easier filtration of the reservoir fluid, which results in higher flow rate.

Exploitation of the reservoir at a constant pressure value at the wellhead with decreasing reservoir pressure leads to a gradual decrease in well deliverability, limiting its productivity over time. Therefore, in order to maintain production at the required level, the wellhead pressure must also be gradually reduced. In turn, the minimum value of the wellhead pressure is dependent on the parameters of the gas received from the natural gas plant. In the variant calculations for the construction of the well deliverability curves, three different wellhead pressures were assumed: 30 MPa, 20 MPa, 12 MPa. The highest well deliverability was obtained for the lowest pressure at the wellhead of 12 MPa, at which the difference between the reservoir pressure and the wellhead pressure is the largest.

The diameter of the well tubing also has a significant impact on the productivity of the well, which translates into pressure loss during gas flow in the pipe and consequently into the flow rate. Two tubing diameters were assumed in the calculations: 3 1/2 in and 2 7/8 in. For a larger diameter of the tubing, the flow resistance is smaller, which means that the pressure loss during flow is smaller and consequently the well deliverability is higher. However, from the point of view of liquid unloading from the bottom of the well, with a smaller diameter of the tubing's, the gas flow rate is higher and the conditions for extracting the liquid phase from the well are more favorable. This is particularly important in the final phase of reservoir exploitation when the reservoir pressure is low and more water flows into the well, as well as condensate drops from the gas.

A comparative analysis of single-phase gas flow variants was carried out and two-phase mist (gas – condensate) in the well showed that, in the case of two-phase flow, the resistance to fluid flow in the well is higher, which is associated with a greater pressure loss caused by higher flow resistance and higher pressure of the fluid column in the well, which in turn translates into a decrease in the productivity of the well.

Author contributions: Conceptualization, formal analysis, methodology J.B., writing – review and editing, writing – original draft preparation, and investigation, I.D.; supervision, validation, project administration, J.B. All of the authors have read and agreed to the published version of the manuscript.

Funding: This research received no external funding.

Conflicts of Interest: The authors of this paper declares no conflicts of interest.

References

[1] Nieć M.: *Hydrocarbon resources classification: Polish, PRMS, UNFC and applied to shale gas. A comparison*. Nafta-Gaz, 9, 2016, pp. 715–716.
[2] Wolan M.: *Technical and technological solutions for the final equipment of wells with a deviated and horizontal section in wells in the Polish Lowlands*. Nafta-Gaz, 8, 2021, pp. 532–535.
[3] Guo B.: *Well Productivity Handbook*. University of Louisiana at Lafayette, Lafayette, LA, United States, 2019.
[4] *High nitrogenous natural gas*, https://www.pgi.gov.pl/en/1239-surowce/surowce/energetyczne/13954-high-nitrogenous-natural-gas.html [10.03.2025].
[5] Dake L.P.: *Fundamentals of Reservoir Engineering.* Elsevier, 1978.
[6] Nagy N. (red.): *Vademecum gazownika, T. 1: Podstawy gazownictwa ziemnego: pozyskiwanie, przygotowanie do transportu, magazynowanie.* Stowarzyszenie Naukowo-Techniczne Inżynierów i Techników Przemysłu Naftowego i Gazowniczego, Kraków 2014.
[7] Hagoort J.: *Fundamentals of Gas Reservoir Engineering*. Elsevier Science, 2012.
[8] Blicharski J.: *Modelowanie analityczne procesu magazynowania gazu w częściowo sczerpanych złożach gazu ziemnego – wybrane zagadnienia*. Wydawnictwa AGH, Kraków 2018.